(12) INTERNATIONAL APPLICATION PUBLISHED UNDER THE PATENT COOPERATION TREATY (PCT)

(19) World Intellectual Property Organization
International Bureau

(43) International Publication Date
14 November 2013 (14.11.2013)

WIPO | PCT

(10) International Publication Number
WO 2013/170103 A1

(51) **International Patent Classification**:
H01M 6/04 (2006.01) *H01L 39/22* (2006.01)

(21) **International Application Number**:
PCT/US2013/040451

(22) **International Filing Date**:
9 May 2013 (09.05.2013)

(25) **Filing Language**: English

(26) **Publication Language**: English

(30) **Priority Data**:
61/644,823 9 May 2012 (09.05.2012) US

(71) **Applicant**: **NORTHWESTERN UNIVERSITY** [US/US]; 633 Clark Street, Evanston, IL 60208 (US).

(72) **Inventors**: **GRZYBOWSKI, Bartosz. WARREN, Scott. YAN, Yong.**

(74) **Agents**: **CELANDER, Daniel, W.** et al.; Klintworth & Rozenblat IP LLC, 850 West Jackson Blvd., Suite 525, Chicago, IL 60607 (US).

(81) **Designated States** *(unless otherwise indicated, for every kind of national protection available)*: AE, AG, AL, AM, AO, AT, AU, AZ, BA, BB, BG, BH, BN, BR, BW, BY, BZ, CA, CH, CL, CN, CO, CR, CU, CZ, DE, DK, DM, DO, DZ, EC, EE, EG, ES, FI, GB, GD, GE, GH, GM, GT, HN, HR, HU, ID, IL, IN, IS, JP, KE, KG, KM, KN, KP, KR, KZ, LA, LC, LK, LR, LS, LT, LU, LY, MA, MD, ME, MG, MK, MN, MW, MX, MY, MZ, NA, NG, NI, NO, NZ, OM, PA, PE, PG, PH, PL, PT, QA, RO, RS, RU, RW, SC, SD, SE, SG, SK, SL, SM, ST, SV, SY, TH, TJ, TM, TN, TR, TT, TZ, UA, UG, US, UZ, VC, VN, ZA, ZM, ZW.

(84) **Designated States** *(unless otherwise indicated, for every kind of regional protection available)*: ARIPO (BW, GH, GM, KE, LR, LS, MW, MZ, NA, RW, SD, SL, SZ, TZ, UG, ZM, ZW), Eurasian (AM, AZ, BY, KG, KZ, RU, TJ, TM), European (AL, AT, BE, BG, CH, CY, CZ, DE, DK, EE, ES, FI, FR, GB, GR, HR, HU, IE, IS, IT, LT, LU, LV, MC, MK, MT, NL, NO, PL, PT, RO, RS, SE, SI, SK, SM, TR), OAPI (BF, BJ, CF, CG, CI, CM, GA, GN, GQ, GW, ML, MR, NE, SN, TD, TG).

Published:

— *with international search report (Art. 21(3))*

— *before the expiration of the time limit for amending the claims and to be republished in the event of receipt of amendments (Rule 48.2(h))*

WO 2013/170103 A1

(54) **Title**: NANOPARTICLE ELECTRIDES

(57) **Abstract**: Disclosed herein are novel electrical materials that are derived from metallic nanoparticle compositions. The nanoparticles are designed such that they have several unexpected properties in response to an applied voltage (for example, non-linear dependence of conductivity as a function of applied voltage and a negative Arrhenius activation energy). The highly versatile nature of these materials and their robust stability at room temperature in the atmospheric conditions provide advantages in nano-scale applications.

NANOPARTICLE ELECTRIDES

CROSS-REFERENCE TO RELATED APPLICATIONS

[01] This application claims benefit of priority under 35 U.S.C. 119 to U.S. provisional patent application serial number 61/644,823 filed May 9, 2012, and entitled "NANOPARTICLE ELECTRIDES," the contents of which is herein incorporated by reference in its entirety.

STATEMENT REGARDING FEDERALLY SPONSORED RESEARCH OR DEVELOPMENT

[02] This invention was made with government support under DE-SC0000989 awarded by the U.S. Department of Energy. The government has certain rights in the invention.

FIELD OF THE INVENTION

[03] The invention relates generally to electrically conductive nanoparticle compositions and their use as materials in electrically active elements such as electrodes, electronic components and electrically conductive devices.

BACKGROUND

[04] Materials with properties that depend on applied voltage are essential components of industrially relevant devices, such as electronic materials (e.g., transistors and sensors), electrochromic materials (e.g., windows), electrocatalysts (e.g., in fuel cells), and magnetic devices (e.g., some classes of memory storage devices). Though extant materials possess properties for performing functions in these material categories, there is a continual search for new materials that may outperform, provide better value than, or provide additional functionality over these materials.

[05] Diodes, transistors, and circuits derived from the combination of these electronic materials have enabled the enormous advances in high impact technology areas, including information processing, computing, molecular electronics, aerospace technologies, and medical technologies. These devices have been constructed from semiconductors—principally silicon—because the p-n junctions that define charge transport can be fabricated with exceptional reliability at a low cost while achieving ever-increasing performance

characteristics. In these devices, the role of metals has been principally relegated to that of electronic interconnects because unlike a p-n junction, which exhibits non-linear current-voltage (i-v) characteristics, metallic materials exhibit Ohmic (linear) behavior. Even at the nanoscale level—whether as nanosheets, nanowires, or nanoparticles—metals and materials having metallic character retain their linear current-voltage characteristics and therefore act as a current carrier with constant resistance under typical operating conditions.

[06] For the foregoing reasons, there is a need for additional compositions and methods for providing novel functionalities and attributes.

BRIEF SUMMARY

[07] In a first respect, an electrochemical cell is provided that includes a plurality of electrodes and an electrolyte. The electrolyte includes a water content comprising from about 0.2 (vol %) to about 5.0 (vol %) and a metallic nanoparticle-SAM composition comprising one member selected from the group having the structure of formula (**I**):

[08] $\underline{W}\text{-}\underline{X}_a\text{-}\underline{Y}\text{-}\underline{Z}_b$ (**I**),

[09] wherein **W** is a metallic nanoparticle, **X** is a metallic nanoparticle-binding moiety, **Z** is a non-dissociative cationic moiety having at least one dissociative anion counterion, ***a*** is an integer selected from 1 to 4, ***b*** is an integer selected from 1 to 30, and **Y** is a linker comprising a covalent bond or a moiety radical having the structure of formula (**II**):

[010] $\text{-}(\underline{Q})_{n'}\text{-}$ (**II**),

[011] wherein **Q** is an element radical selected from the group of elements consisting of C, N, O, P, S, Si and combinations thereof and ***n'*** is an integer selected from 1 to 30. The conductivity of the electrochemical cell decreases with increasing temperature.

[012] In a second respect, the use of the electrochemical cell as described above is provided in a device configured to operate within a range of relative humidity from about 20% to about 80%, wherein the device is selected from a transistor and a thermistor.

[013] In a third respect, a nanoscale switch is provided that includes an electrolyte composition comprising a nanoparticle composition and a water content comprising from about 0.2 (vol %) to about 5.0 (vol %). The nanoparticle composition includes a metallic nanoparticle and a ligand having a non-dissociative cationic moiety and a dissociative anion counterion moiety, wherein the ligand is coupled to the metallic nanoparticle. The nanoparticle composition is configured to switch between a first state and a second state, wherein electron movement in the nanoparticle composition is permitted when the switch is in the first state and wherein electron movement in the nanoparticle composition is not

permitted when the switch is in the second state.

[014] These and other features, objects and advantages of the present invention will become better understood from the description that follows. In the description, reference is made to the accompanying drawings, which form a part hereof and in which there is shown by way of illustration, not limitation, embodiments of the invention.

BRIEF DESCRIPTION OF THE DRAWINGS

[015] The features, objects and advantages other than those set forth above will become more readily apparent when consideration is given to the detailed description below. Such detailed description makes reference to the following drawings.

[016] **FIG. 1A** shows a schematic of a thin film of ligand-stabilized gold nanoparticles is in contact with two gold electrodes of an electrochemical cell. The device is not drawn to-scale; the nanoparticle has at least one dimension from about 6 to about 8 nm, the film is about 0.1 to about 1 μm thick and gap between electrodes is about 50 to about 500 μm. When a voltage (+, -) is applied to the electrical leads, chloride ions move towards the positive electrode.

[017] **FIG. 1B** shows a schematic of a depletion of chloride ions creates anion vacancy sites adjacent to ammonium cations. These cations capture unpaired electrons (small blue spheres) that exist within the SAM and electrostatically stabilize them as polarons (glowing small blue spheres). The unpaired polaron electrons are in equilibrium with paired bipolaron electrons (glowing large blue spheres) via the reaction $2\ e^- \leftrightarrows e_2^{2-}$.

[018] **FIG. 1C** shows preferred embodiments for a SAM material found in formula (**Ia**) present in the metallic nanoparticle-SAM composition.

[019] **FIG. 2A** depicts steady-state *j-V* characteristics for a two-electrode device. TMA alkanethiols with chain lengths of 5, 8, or 11 methylene units were used for SAM [formula (**IIa**) Y-Z]: $S\text{-}(CH_2)_n\text{-}N(CH_3)_3^+Cl^-$, where n = 5 (denoted by squares), 8 (denoted by circles), or 11 (denoted by triangles). The current densities correspond to electrical conductivities of 10^{-8} to 10^{-6} S/cm.

[020] **FIG. 2B** illustrates the device geometry used in the four electrode measurement.

[021] **FIG. 2C** depicts the steady-state j-V characteristics for a four-electrode device of FIG. 2B, wherein the metallic nanoparticle-SAM included a TMA ligands with 11 methylene units (SAM of formula (**IIa**) [Y-Z]: $S\text{-}(CH_2)_{11}\text{-}N(CH_3)_3^+Cl^-$) and the device had a *sensing* electrode width of 500 μm, a gap between *sensing* electrodes of 500 μm, and a gap between *test* electrodes of 2.5 mm. The *test* voltage was varied from 0 to 4 V while the *sensing*

voltage was maintained at 0.2 V.

[022] **FIG. 2D** depicts time-of-flight secondary ion mass spectrometry (ToF-SIMS) was used to map the elemental distributions within the nanoparticle film between positive (+) and negative (-) electrodes. The electrodes are shown in the x-y plane as gold-colored triangles and have a gap size of 50 μm. The grid lines in the x-y plane are drawn every 20 μm. The distribution of gold is constant across the device and is used as a reference against which changes in sulfur (S).

[023] **FIG. 2E** depicts the same experimental setup as FIG. 2D, except that the distribution of gold is constant across the device and is used as a reference against which changes in chloride (Cl).

[024] **FIG. 2F** depicts the change in the ratio of the denoted element ("x") relative to gold (Au), where x = Cl (squares) or S (triangles). The gradient in Cl increased linearly with voltage while S did not change. This experiment was performed with gold electrodes while those of **FIGs. 2A-E** were performed with gold-silica composite electrodes.

[025] **FIG. 2G** depicts a plot of gold distribution between two electrodes. The nanoparticle film was polarized at 4 V for 10 minutes. The electrodes were spaced 50 μm apart.

[026] **FIG. 2H** illustrates an SEM image of C_{11}-TMA AuNPs.

[027] **FIG. 2I** depicts the geometry of the electrode pattern used in the four-electrode device.

[028] **FIG. 3A** depicts an Arrhenius plot of the steady state current density vs. the thermal energy shows that heating decreases current transport and that the apparent activation energy is negative with a value of -0.9 eV.

[029] **FIG. 3B** depicts a model for electron transfer in which there exists a species within the SAM that switches between a conductive, low-energy "*on*" state and a less-conductive, high-energy "*off*" state. As the temperature is increased, the switch spends a larger proportion of its time in the high energy state, leading to a decrease in electrical conductivity.

[030] **FIG. 3C** illustrates a Free energy profile along the reaction coordinate. The activation energy to go from the *on* state to the *off* state is 0.9 eV.

[031] **FIG. 3D** illustrates Magnetic force microscopy (MFM) measurements for several types of thin films. The scan size for all images is 8 μm by 40 μm. The gap between electrodes is 50 μm. Each scan is performed from the top to the bottom; the voltage is increased halfway through each image, as marked by the dashed white line.

[032] **FIG. 3E** illustrates in section (**Ia**) MFM image of a film composed of gold nanoparticles with C_{11} TMA ligands (see FIG. 1C). The phase scale bar is from 25° to 45°.

In section **(IIa)**, MFM image of a film composed of gold nanoparticles with 11-mercaptoundecanoic acid. The phase scale bar is from 40° to 90°. In section **(iii)**, MFM image of a continuous gold film. A current was passed that was 1000 times higher than those passed with the nanoparticle films. The phase scale bar is from 90° to 100°.

[033] **FIG. 3F** depicts the change in phase is plotted (squares) as a function of voltage for the nanoparticles with charged ligands, showing that $\Delta\phi \sim V^2$. The control experiment from **ii** is plotted as triangles.

[034] **FIG. 4A** depicts the presence of unpaired electrons exist in image potential states within the SAM. Immediately after subjecting the nanoparticle film to an applied potential (V), chloride ions move capacitively (red arrows). The unpaired electrons become electrostatically trapped at the chloride vacancy sites (blue arrows).

[035] **FIG. 4B** illustrates the case wherein two unpaired electrons are trapped at nearby cationic sites, a paired electron species—that is, a bipolaron—may form.

[036] **FIG. 4C** depicts scaling the film resistance (R) by the ligand length (L) indicates a hopping mechanism for electron transport.

[037] **FIG. 4D** depicts an energy diagram of two adjacent nanoparticles and their SAMs. The electron/bipolaron (e^-/ee^{2-}) redox couple mediates electron transfer between the nanoparticles. The free energy of the e^-/ee^{2-} redox couple can be described by a reaction coordinate diagram according to Marcus theory (**FIG. 3D**). The parabolic energy surface of the diagram implies that the electron density of states (DOS) have Gaussian distributions. The electrons at higher energies are stabilized only by image charges and are not trapped at chloride ion vacancy sites.

[038] **FIG. 4E** depicts one preferred embodiment wherein materials are mesoscopic analogues to electrides. The nanoparticle core and ligand (grey) are positively charged while the solvated electrons and chloride ions (purple) are negatively charged.

[039] **FIG. 5A** depicts the typical layout for a transistor. There are three gate electrodes; the middle gate electrode is biased with respect to the outer electrodes. Between the gate electrodes are the source (S) and drain (D) electrodes. The nanoparticle film is deposited across all 5 electrodes (red film). The voltage between source and drain was held constant (for example, 2V in **Fig. 5B**) and the current between the source and drain was measured as the gate voltage was increased. The on/off ratio (Ion/Ioff) of the transistor is defined as the current at the indicated gate voltage (Ion) divided by the current when no gate voltage is applied (Ioff). In this device, as the gate voltage is increased, the current between the source

and drain is modulated.

[040] **FIG. 5B** depicts a plot of the electrical characteristics of the device shown in **FIG. 5A**, which can be described by a second-order polynomial, thereby demonstrating that the material's conductivity increases linearly with the gate voltage. The conductivity of the nanoparticle film has increased by a factor of 250 at an applied potential of 30 V, thereby providing an on/off ratio for the transistor of 250.

[041] **FIG. 5C** depicts a graphical representation of resistance as a function of temperature for a thermistor device containing the metallic nanoparticle-SAM composition of formula (**Ia**).

[042] **FIG. 5D** illustrates a diode containing a first deposition of metallic nanoparticles of formula (**Ia**) and a second deposition of metallic nanoparticles having a structure different from formula (**Ia**).

[043] **FIG. 5E** depicts the structures of the metallic nanoparticles of the device shown in **FIG. 5D**.

[044] **FIG. 5F** illustrates a graphical representation of the resultant composition and structure of **FIGs. D** and **E.**

[045] **FIG. 6** illustrates a flexible substrate contain transistors having the metallic nanoparticle-SAM compositions described herein (circled elements of circuit).

[046] **FIG. 7** depicts the synthetic reaction scheme for several preferred embodiments of formula (**Ia**).

[047] While the present invention is amenable to various modifications and alternative forms, exemplary embodiments thereof are shown by way of example in the drawings and are herein described in detail. It should be understood, however, that the description of exemplary embodiments is not intended to limit the invention to the particular forms disclosed, but on the contrary, the intention is to cover all modifications, equivalents and alternatives falling within the spirit and scope of the invention as defined by the embodiments above and the claims below. Reference should therefore be made to the embodiments and claims herein for interpreting the scope of the invention.

DETAILED DESCRIPTION

[048] The compositions and methods now will be described more fully hereinafter with reference to the accompanying drawings, in which some, but not all permutations and variations of embodiments of the invention are shown. Indeed, the invention may be embodied in many different forms and should not be construed as limited to the embodiments

set forth herein. These embodiments are provided in sufficient written detail to describe and enable one skilled in the art to make and use the invention, along with disclosure of the best mode for practicing the invention, as defined by the claims and equivalents thereof.

[049] Likewise, many modifications and other embodiments of the compositions and methods described herein will come to mind to one of skill in the art to which the invention pertains having the benefit of the teachings presented in the foregoing descriptions and the associated drawings. Therefore, it is to be understood that the invention is not to be limited to the specific embodiments disclosed and that modifications and other embodiments are intended to be included within the scope of the appended claims. Although specific terms are employed herein, they are used in a generic and descriptive sense only and not for purposes of limitation.

[050] Unless defined otherwise, all technical and scientific terms used herein have the same meaning as commonly understood by one of skill in the art to which the invention pertains. Although any methods and materials similar to or equivalent to those described herein can be used in the practice or testing of the present invention, the preferred methods and materials are described herein.

[051] Moreover, reference to an element by the indefinite article "a" or "an" does not exclude the possibility that more than one element is present, unless the context clearly requires that there be one and only one element. The indefinite article "a" or "an" thus usually means "at least one."

[052] As used herein, "about" means within a statistically meaningful range of a value or values such as a stated concentration, length, molecular weight, pH, sequence identity, time frame, temperature or volume. Such a value or range can be within an order of magnitude, typically within 20%, more typically within 10%, and even more typically within 5% of a given value or range. The allowable variation encompassed by "about" will depend upon the particular system under study, and can be readily appreciated by one of skill in the art.

[053] Novel nanoparticle materials termed nanoparticle electrides and having unusual charge transport characteristics are provided. In current density-voltage (j-V) measurements employing a two-electrode device containing certain liganded metallic nanoparticle compositions (**FIG. 1**), it was discovered that the novel materials display a steady state current density that increases approximately as V^3 ($j \sim V^3$) (**FIG. 2A**), indicating that the electrical conductivity of the materials depends upon the applied voltage. This unusual electronic behavior was confirmed using a four-electrode device containing the materials, wherein two electrodes were configured as “test” electrodes for varying voltage potential

between them and wherein the current was measured using two orthogonally-related "sensing" electrodes (**FIG. 2B**). As the voltage was varied from 0 to 4 V, the steady-state sensing current density was determined to increased as a function of the square of the test voltage ($j_{sense} \sim V_{test}^2$) in the four-electrode devices (**FIG. 2C**). This resultant behavior is consistent with the noted observation that $j \sim V^3$ in the two-electrode devices owing to the fact that voltage increases the electric field (E ~ V) in the direction that the carriers move. These two electrode device configurations also demonstrated that contact resistance effects are small to negligible for these materials. By increasing the applied voltage or by modifying the device geometry, even larger changes in conductivity can be obtained. Conductivity can be increased by many orders of magnitude in these materials through the application of a small voltage.

[054] These properties are surprisingly unexpected for the disclosed materials, as prior art materials made from ligand-stabilized metal nanoparticles have room temperature conductivities that are invariant with voltage and therefore exhibit linear *j-V* characteristics. Prior art nanoparticle materials typically used in high current density applications are also limited due their low electrical conductivity. These novel materials and their properties – as well as devices and nanoscale, energy-gated, switches that include these materials – are described in greater detail below.

Nanoparticle electride materials

[055] Nanoparticle electride materials are composed of metallic nanoparticles functionalized with a self-assembled monolayer (SAM). The nanoparticles can be metal nanoparticles, wherein the metal is selected from Au, Ag, Pt, Cu, Co, Ni, Fe, Mn, Ru, among others. Such metal nanoparticle compositions can be prepared by reduction of metal salts (for example, $HAuCl_4$, $AgNO_3$, $AgClO_4$, $Ag(CH_3CO_2)$, $PtCl_4$, $PdCl_4$, $Cu(CH3CO_2)_2$, $CoCl_2$, $Co(CH_3CO_2)_2$, $Ni(CH_3CO_2)$ and Ni(acetylacetone)$_2$) in one-phase or two-phase solutions in the presence of a stabilizer. For example, one-phase nanoparticle synthesis can be accomplished with the reduction of aqueous $HAuCl_4$ by citrate. For example, two-phase nanoparticle synthesis can be accomplished by transferring aqueous metal salts to a toluene solution containing long-chain alkylammonium bromide surfactants. After isolation of the organic phase, capping agents, such as alkanethiols, are added to the solution, followed by the addition of an aqueous solution of reducing agents to promote nucleation of the nanoparticles having a size range from about 1 nm to about 3 nm. The reducing agents can NaBH4, hydrazine, sodium citrate, potassium bitatrate, dimethyl formamide, ascorbic acid, superhydrides, amines, alcohols, and polyalcohols. Weak reducing agents provide small

nanoparticles, while strong reducing agents provide large nanoparticles. In the absence of capping agents the two-phase method yields larger nanoparticles ranging in size from about 5 nm to about 8 nm stabilized by the alkylammonium bromide surfactants. Accordingly, the inclusion of capping agents permit the isolation of resulting nanoparticles stabilized by a shell of capping ligands as a powder.

[056] One can control the size, shape, and polydispersity of metal nanoparticles obtained by the metal salt reduction method by varying reaction parameters, such as the concentration and/or structure of capping agents and the selection of reducing agent used, among others. Post-reaction size-selection procedures can be used to isolate specific size classes of nanoparticles, such as size-selective precipitation techniques, heating, etching, annealing and chromatography, all of which are well understood in the art.

[057] Other methods for synthesizing metal nanoparticles include sequestering and subsequently reducing metal ions (for example, Au^{3+}, Pt^{2+}, Pd^{2+}, Ni^{2+}, Mn^{2+}, Cu^{2+}, Fe^{3+} and Ru^{3+}) in dendrimers, reducing metal ions in reverse micelles, and thermally-decomposing metal-carbonyl compounds (for example, $Co_2(CO)_8$ and $Fe(CO)_5$) in the presence of surfactants (for example, tributylphosphine).

[058] Preferred sizes of nanoparticle electrides range from about 1 nm to about 100 nm, wherein highly preferred sizes having at least one dimension ranging from about 2 nm to about 25 nm. The preferred method for synthesizing metal nanoparticle electrides include a novel modification of the aforementioned two-step metal reduction procedure for preparing metal nanoparticles. In the preferred process, an initial synthesis of nanoparticles having at least one dimension ranging from about 2 nm to about 4 nm ("2-4 nm material") is performed using borohydride as reducing agent. Subsequently, nanoparticles having at least one dimension ranging from about 5 nm to 8 nm is prepared in which the nanoparticles synthesis is achieved using a variation of the initial procedure used to prepare the 2-4 nm material. The reducing agent is hydrazine rather than borohydride for the second synthesis, and a portion of the 2-4 nm material serves as seed material for growing larger nanoparticles. In both procedures, the resultant nanoparticles are stabilized by a shell of alkylamine caps. **Example 1** provides details of this procedure.

[059] In addition to metal nanoparticles, the nanoparticle electrides can also include semiconductor nanoparticles, such as binary semiconductors. Preferred examples of binary semiconductors denoted as ME (for example types II-VI, III-V II and IV-VI) include ME (type II-VI), where M is preferably Zn, Cd or Hg, and E is preferably S, Sc or Te; ME (type III-V), where M is preferably In and Ga and E is As and P, and ME (type IV-VI), where M is

preferably Pb and Sn and E is preferably Se, S and Te). Other preferred examples of semiconductor nanoparticles include core-shell semiconductor nanoparticles (type I, reverse type I, type II among others). Preferred examples of type I core-shell semiconductor nanoparticles include CdSe/CdS, CdSe/ZnS and InAs/CdSe. Preferred examples of reverse type I core-shell semiconductor nanoparticles include CdS/HgS, CdS/CdSe and ZnSe/CdSe. Preferred examples of type II core-shell semiconductor nanoparticles include ZnTe/CdSe, CdTe/CdSe and CdS/ZnSe. Other preferred examples of semiconductor nanoparticles include metal oxides, such as FeO, Fe_2O_3, NiO, EuO, TiO_2, CuO, Cu_2O, UO_2, UO_3, Bi_2O_3, SnO_2, Sb-doped SnO_2, F-doped SnO_2, indium tin oxide (ITO), $BaTiO_3$, $LiNbO_3$ MoO_3, Nb_2O_5, Ta_2O_5, or WO_3.and La_2CuO_4. Still other preferred examples of semiconductor nanoparticles include EuS, $CrBr_3$, BiI_3, HgI_2, TiBr, Se, PtSi, FeS_2, AgS_2, As_2S_3, $AnSiP_2$, $AgGaS_2$, $CuInSe_2$, Cu_2ZnSnS_4.

[060] Highly preferred metallic nanoparticles include as their metallic component one of the following: SnO_2, F-doped SnO_2, indium tin oxide (ITO), Sb-doped SnO_2, Fe_2O_3, TiO_2, MoO_3, Nb_2O_5, Ta_2O_5, or WO_3.

[061] Procedures for synthesizing semiconductor nanoparticles is well known in the art, including methods based upon pyrolysis of organometallic precursors in coordinating solvents, such as a mixture of long-chain alkylphosphines, alkylphosphine oxides, alkylamines, among others. For example, CdSe nanoparticles can be synthesized by quickly injecting a mixture of selenium and dimethylcadmium dissolved in trioctylphosphine into hot (~300 °C) trioctylphosphine oxide and subsequently reducing the temperature ((~250 °C) to promote growth of the nanoparticles.

[062] As used herein in the context of the nanoparticle electride compositions disclosed herein, "metallic nanoparticles" include metal nanoparticles, semiconductor nanoparticles and carbon-based materials (for example, carbon black, fullerenes, carbon nanotubes, graphene and metal carbides).

[063] Preferably, the metallic nanoparticle-SAM composition comprises one member selected from the group having the structure of formula (**I**):

[064] $\underline{W}\text{-}\underline{X}_a\text{-}\underline{Y}\text{-}\underline{Z}_b$ (**I**),

[065] wherein **W** is a metallic nanoparticle, **X** is a metallic nanoparticle-binding moiety, **Z** is a non-dissociative cationic moiety having at least one dissociative anion counterion, ***a*** is an integer selected from 1 to 4, ***b*** is an integer selected from 1 to 30, and **Y** is a linker comprising a covalent bond or a moiety radical having the structure of formula (**II**):

[066] $\text{-}(\underline{Q})_{n'}\text{-}$ (**II**),

[067] wherein **Q** is an element radical selected from the group of elements consisting of C, N, O, P, S, Si and combinations thereof and ***n***' is an integer selected from 1 to 30. As used herein the individual moieties **-Q-** are independent and distinct from each other in formula (**II**). Thus, the formula (**II**) encompasses both homo-polymers and mixed polymers of **-Q-**.

[068] The conductivity of said electrochemical cell decreases with increasing temperature. The novel attributes of these materials is evident when the composition contains a water content in the range from about 0.2 (vol %) to about 5.0 (vol %).

[069] More preferably, the metallic nanoparticle-SAM materials have the structure of formula (**Ia**):

[070] **W-X-Y-Z**$_b$ (**Ia**),

[071] where **W** is a metallic nanoparticle, **X** is a metallic nanoparticle-binding moiety; **Z** is a non-dissociative cationic moiety having at least one dissociative anion counterion and ***b*** is an integer selected from 1 and 30; and **Y** is a linker comprising a covalent bond or a moiety radical having the structure of formula (**IIa**):

[072] $-(CR^1R^2)_n-$ (**IIa**),

[073] where R^1 and R^2 are each independently from another selected from hydrogen, halo, hydroxy, saturated or unsaturated C_{1-6} alkyl, substituted or unsubstituted C_{1-6} alkyl, saturated or unsaturated C_{1-6} alkyloxy, substituted or unsubstituted C_{1-6} alkyloxy, substituted or unsubstituted phenyl, amino, amide, ester, ether, acyl, carboxyl, keto, thiol, silyl, silyl ether, siloxyl, saturated or unsaturated heterocycle selected to contain one or more heteroatoms selected from O, S, N, P, wherein said saturated or unsaturated heterocycle is substituted with one or more substituents each independently from another selected from halo, hydroxy, saturated or unsaturated C_{1-6} alkyl, substituted or unsubstituted C_{1-6} alkyl, saturated or unsaturated C_{1-6} alkyloxy, substituted or unsubstituted C_{1-6} alkyloxy, substituted or unsubstituted phenyl, amino, amide, ester, ether, acyl, carboxyl, keto, thiol, and wherein ***n*** is an integer from 0-30. As used herein the individual moieties of **-CR^{1}R^2-** are independent and distinct from each other in formula (**IIa**). Thus, the formula (**IIa**) encompasses both homo-polymers and mixed polymers of **-CR^{1}R^2-**.

[074] Preferably, order of preference for structures of **Y** having formula (**IIa**) increases with decreasing ***n***. Thus, the lower number of inter-carbon subunits (that is, the number of linearly-linked carbons separating **X** and **Z**) found in the formula (**IIa**) of **Y** are preferred for inclusion in SAM materials according to formula (**Ia**) relative to a higher number of inter-carbon subunits. This feature is preferred because higher conductivity is associated with shorter lengths of formula (**Ia**). Preferred, minimal lengths for **Y**-**Z** fall within the range from

less than about 0.8 nm to less than about 2.5 nm.

[075] Preferably, **X** is any moiety that provides stable binding of the SAM to the nanoparticle surface. Examples of preferred moieties for **X** having stable binding to metal nanoparticles include amine, thiol, phosphane, phosphine, carboxylate, dithiocarbamate, xanthanate, among others. Examples of preferred moieties for **X** having stable binding to semiconductor nanoparticles include phosphine, phosphine oxide, phosphite, phosphate, carboxylate, phthalimide, acetylacetone, pyridine, 1,2-dihydroxyphenyl, among others.

[076] Preferably, the non-dissociative cationic moiety of **Z** can be ammonium, phosphonium, pyridinium, imidazolium, among others. Preferably, the dissociative anion counterion of **Z** can be fluoride, chloride, bromide, iodide, sulfate, phosphate, chlorate, chlorite, nitrite, nitrate, hydroxide, sulfide, hydrosulfide, carbonate, bicarbonate, acetate, thioacetate, among others. The preferred forms of **Z** thus include salts having 1+/1- and 2+/2- ionized charge states. Highly preferred forms of **Z** include salts where the dissociative anion counterion has an effective size not greater than one-half the effective diameter of the interstitial spaces between functionalized nanoparticles having a SAM when assembled onto a substrate. This is due to the requirement for movement of the dissociative anion counterion in the nanoparticle electride upon application of a voltage to the material.

[077] Preferred SAM ligand moieties in formula (**Ia**) (for example, the **X-Y-Z** portion) are those that have two or more of the following chemical features: **X** is an amine or thiol; **Y** is an alkyl moiety of formula (**IIa**), and **Z** is a salt composed of a non-dissociative tertiary amine cation counterion and halide dissociative anion counterion. More preferred SAM's include compounds of formula (**Ia**) that have two or more of the following chemical features: **X** is a thiol; **Y** is an unsubstituted C_{1-20} alkyl moiety of formula (**IIa**), and **Z** is a salt composed of a tertiary amine and halide dissociative anion counterion. Highly preferred SAM's include compounds of formula (**Ia**) that have two or more of the following chemical features: **X** is a thiol; **Y** is an unsubstituted C_{3-12} alkyl moiety of formula (**IIa**) (that is, having ***n*** = 3 to 12), and **Z** is a salt composed of a trialkylammonium cation and halide dissociative anion counterion. Most preferred SAM's include compounds of formula (**Ia**) that have the following chemical features: **X** is a thiol; **Y** is an primary C_{4-11} alkyl moiety of formula (**IIa**) (that is, having ***n*** = 4 to 11), and **Z** is a salt composed of a trimethylammonium halide, wherein halide is chloride and bromide.

[078] Without being limited to the foregoing highly preferred embodiments of formula (**Ia**), additional highly preferred embodiments of formula (**Ia**) include formula (**IIa**) that have the following structural features for **Z**: (a) with respect to the non-dissociative cationic moiety,

highly preferred species include ammonium, imidazolium, pyridinium, phosphonium, pyrazolium, pyrrolidinium, sulfonium, sulfonyl imide, piperidinium, morpholinium, and cyclopropenylium; and (b) with respect to the dissociative anion counterion, highly preferred species include chloride, bromide, iodide, nitrate, thiocyanate, acetate, and tetrafluoroborate. Most optimally, the cations that meet both of these criteria include ammonium, imidazolium, pyridinium, phosphonium, pyrazolium, pyrrolidinium, sulfonium, sulfonyl imide, piperidinium, morpholinium, and cyclopropenylium.

[079] Exemplary SAM ligands in formula (**Ia**) are those that fall within the highly preferred group include C_5- C_8- and C_{11}-alkanethiol ligands end-functionalized with trimethylammonium chloride (see, for example, **FIGs. 1** and **7**). **Example 1** provides representative synthesis of these compounds. **Example 2** provides a representative preparation of Au nanoparticles capped with dodecylamine and the ligand exchange replacement method for generating the nanoparticles functionalized with SAM's corresponding to C_5- C_8- and C_{11} alkanethiol ligands.

[080] The synthesis of the metallic nanoparticle-SAM compositions embodying formulas **I**, **Ia**, **II**, and **IIa** are well known in the art. Exemplary synthesis schemes are provided in the Examples.

[081] The metallic nanoparticle-SAM's can be deposited onto a substrate in a variety of ways, including the use of drop-casting, spin-coating, vapor-phase deposition, among others. Preferred substrates include those having compositions having carbon-coated materials, graphite, silicon-nitride, metal, glass, silicon-oxide. Where the substrates are electrodes (for example, lithographically-patterned electrodes), preferred substrates include metal nanocomposite or metal-silica nanocomposite. In the example where the electrodes have Au as the metal, the primary distinction between the two types of electrodes is that Au-silica electrodes have a higher capacitance than Au electrodes. The deposited metallic nanoparticle-SAM film should provide at least one continuous pathway between each electrode. The use of the metallic nanoparticle-SAM's as electrolytes in electrochemical cells is operated preferably in a humidified environment, preferably one that contains a relative humidity in the range from about 20% to about 80%.

[082] The electrodes should be designed to have as high a capacitance as possible. There are multiple approaches for achieving high capacitance electrodes, including the design of an electrode with a high surface area or the selection of an electrode material or materials that provide increased capacitance. The electrode should also be stable under the voltages applied and while in contact with the nanoparticle film. For most experiments, electrodes were

prepared by sequential deposition of 5 nm of Cr, 40 nm of Au, 5 nm of Cr, and 100 nm of SiO_2 onto an insulating substrate such as silica. The electrodes are thermally processed at 700 °C for 10 minutes with rapid heating and cooling rates (30 °C/min.) to/from 700 °C. This provides a nanostructured gold/silica electrode with a capacitance that is approximately 200 times higher than a planar gold electrode but with a comparable electrical conductivity.

[083] An alternate fabrication strategy is to design two substrates, each of which has one or more electrodes. Metallic nanoparticle-SAM films are deposited onto these substrates. The two substrates (with metallic nanoparticle-SAM) are then laminated together, thereby creating a sandwich-like structure comprised of substrate-electrode-nanoparticle film-electrode-substrate. These sandwich structures allow extremely thin layers of metallic nanoparticle-SAM film to be sandwiched between two electrodes, thereby improving material response to the applied voltage.

[084] The resultant films formed on the substrate are preferably continuous firms with a thickness ranging from about 100 nm to about 1 μm. Film assemblies can vary in their form depending upon the assembly/deposition method used, such that the resultant nanoparticle SAM assemblies can exhibit a high degree of order (super-lattices), short-range order, or a high degree of disorder. The preferred deposition method is drop-casting that enables preparation of nanoparticle SAM films on electrode surfaces having an ordered lattice structure (**FIG. 1A, B**).

[085] The charge transport and ion movement properties of the resultant nanoparticle SAMS materials were found to display surprising properties. For these experiments electrochemical cell devices configured a two-electrode systems and four electrode systems were used. Details of these systems are found in **Example 4**. The distribution of elements using secondary ion mass spectroscopy (SIMS) before and after applying a voltage (**FIG. 2D-F**). Prior to applying a voltage, there were no composition gradients. After applying a voltage for hundreds of seconds, there was still no gradient in the distributions of gold (**FIG. 2G**) or sulfur (**Fig. 2D**) because the gold nanoparticles are immobile and the thiols are chemisorbed strongly to the gold nanoparticles. A chloride ion gradient developed, however, with the chloride concentration 10% higher at the positive electrode (**Fig. 2E**). The SIMS analysis allowed us to examine the concentration gradients as a function of voltage (**Fig. 2F**). While the sulfur does not move at any voltage, the chloride ions develop a gradient that increases linearly with voltage.

[086] Additional experiments were conducted that demonstrated that the conductive

behavior of the nanoparticle SAMs materials as a function of applied voltage were not attributed to classical atomic element-based redox chemistry nor to the presence of additional unexpected molecular species as contaminants in the prepared materials. An analysis by SIMS demonstrated that at the 10 ppt level, no elements besides Au, C, H, S. N and Cl were present in the material that could mediate charge transfer via redox reactions. The involvement of oxygen reduction was ruled out as a contributing factor because the electrical characteristics of the materials remained unchanged whether the device was operated in an ambient air or Ar atmosphere. Because the material's conductivity occurs between 0.5-1.0V (**FIG. 2C**), water-mediated redox chemical reactions does not contribute the observed charge transfer phenomenon of the nanoparticle SAMs materials. To determine the contributions of the redox-reactive atomic elements themselves that compose the nanoparticle SAMs materials, an amount of charge was passed through the device that was greater than 100-fold the required amount of current to oxidize or reduce all gold, chloride, sulfur, water and oxygen present in the device (experiment performed under ambient temperature and pressure conditions containing humidified air atmosphere). The preferred device characteristic, namely the $\sigma \sim V^2$ relationship, was maintained before, during and after the experiment. The absence of classical atomic element-mediated redox chemical reactions and the lack of additional molecular species indicates that electron transport is occurring in the nanoparticle SAMs materials under applied voltage conductions.

[087] Highly preferred embodiments of metallic nanoparticle-SAM materials and electrochemical cell devices that include them display high electrical conductivity and retain their preferred $\sigma \sim V^2$ relationship under extraordinary high electric current demand with high electric fields. The integrity and robustness of the prepared devices can be analyzed using the techniques well known in the art, as well as those described herein.

[088] Notwithstanding these preferred embodiments, yet other embodiments have novel properties within the scope of disclosure include mixed metallic nanoparticle compositions and depositions. These materials include at least one metallic nanoparticle-SAM of the formula (**Ia**) and at least one metallic nanoparticle having a structure different from formula (**Ia**). Such materials having mixed metallic nanoparticle compositions and depositions can have modified electrical conductivity and quasi-exponential dependencies that fall between linear $\sigma \sim V$ and the preferred $\sigma \sim V^2$. Such material compositions preferably include multiphasic electrical conductivities as a function of applied voltage.

[089] The foregoing observations indicate that the movement of chloride ions is capacitive

and not Faradaic and that the movement of chloride, sulfur, and gold make no contribution to the steady state current.

Metallic nanoparticle SAMs materials as an energy-dependent sensor

[090] Because the materials possessed two types transport phenomena, chloride ion transport and electron transport, experiments were conducted to determine whether the material's electrical properties could be perturbed under different conditions or in response to certain stimuli. The effect of temperature on the electrical behavior of the nanoparticle SAMs materials was investigated. Unlike traditional charged nanoparticle materials, the steady-state current as a function of applied voltage decreased for nanoparticle SAMs materials as the materials were subjected to increased temperatures. The steady-state current under an applied voltage decreased with temperature, wherein the observed phenomenon displays Arrhenius behavior with a negative activation energy of -0.9eV (**FIG. 3A, C**).

[091] Thus, preferred embodiments of metallic nanoparticle-SAM materials display (**I** and **Ia**) a non-linear conductivity-voltage relation (that is, $\sigma \sim V^2$) and negative Arrhenius activation energies.

[092] In this respect, conductivity of these materials depends very sensitively on temperature. These materials can be used to build what may be among the most sensitive thermometers yet designed. They can detect changes in temperature of as little as 0.0001 °C. For some embodiments of preferred compositions the useful range of temperature can be from about -30 °C to about 150 °C, inclusively; other embodiments can be amenable for use in a temperature range from about -20 °C to about 50 °C, inclusively.

[093] Thus, one preferred embodiment is a nanoscale sensor configured for sensing an external stimulus. The nanoscale sensor includes a nanoparticle composition comprising a metallic nanoparticle and a ligand having a cationic moiety and a dissociative anion counterion moiety, wherein the ligand is coupled to the metallic nanoparticle. The nanoparticle composition provides a first conductivity in response to a first amount of applied voltage. The occurrence of a second conductivity that is lower than the first conductivity at the first applied voltage in the nanoparticle composition is indicative of the presence the external stimulus. The external stimulus can be temperature, radiation, chemical reaction, among others. For temperature sensing, an optimal configuration can be achieved when the nanoparticle thin film is preferably covered in an electrically insulating but thermally conductive thin film. The device can placed in contact with the object that is to be measured by preferably making contact between the electrically insulating/thermally conductive thin

film and the object. For radiation (for example, photonic radiation), the device is oriented to obtain maximum exposure to the radiation source. If a protective coating is placed on top of the nanoparticle film, it preferably transparent to the radiation. For sensing chemical reactions, a protective coating can be preferably omitted from the top surface of the film. A preferred geometry can include placing the device within the chemical medium (for examples, a liquid or a gas) that is to be sensed. This allows the chemical medium to infiltrate into the nanoparticle film.

[094] In another respect, the temperature experiments revealed that the metallic nanoparticle-SAM material include electron transfer between adjacent nanoparticles via switchable state within the SAM (**FIG. 3B**). The switch allows electron transfer in its ground, "*on*" state and prevents electron transfer in its high energy, "*off*" state. Elevated temperature increases the proportion of time the switch spends in its *off* state, lowering the material's conductivity. Within the metallic nanoparticle-SAM films having Au as the metallic nanoparticle and SAM ligand in the formula (**Ia**) consisting of $-S(CH_2)_{11}N(CH_3)_3^+Cl^-$ for SAM, activation energy for switching from the *on* state to the *off* state is 0.9 eV (**FIG. 3C**). Since composition of the metallic nanoparticle-SAM dictates the overall conductivity of the resultant metallic nanoparticle-SAM material, different metallic nanoparticle-SAM compositions can display different activation energies for electron transfer. Accordingly, different nanoswitches having differently tunable sensitivities can be designed simply by varying the metallic nanoparticle-SAM compositions to have particular electrical properties, including unique activation energy for electron transfer.

[095] Thus, one preferred embodiment is a nanoscale switch that includes a nanoparticle composition comprising a metallic nanoparticle and a ligand having a cationic moiety and a dissociative anion counterion moiety, wherein the ligand is coupled to the metallic nanoparticle. The nanoparticle composition is configured to switch between a first state and a second state, wherein electron movement in the nanoparticle composition is permitted when the switch is in the first state and wherein electron movement in the nanoparticle composition is not permitted when the switch is in the second state.

[096] The identity of the switch was determined in the following manner. The SAM ligand, itself was not likely to be the switch because the HOMO and LUMO of the alkanethiol ligands are far from the gold nanoparticle's Fermi level, making it improbable that electron transfer occurs via molecular orbitals. The switch was neither an atom nor a molecule, because no redox reactions of atomic or molecular species in the SAM were demonstrated occur in the metallic nanoparticle-SAM compositions (**FIG. 2D-F**). The materials have anion

vacancy sites (that is, an F-center defect), as suggested the fact that the capacitive movement of chloride ions in the material under an applied voltage creates chloride ion vacancy sites within the SAM. Because the creation of such sites provide an opportunity to trap electrons, the switch was deemed to include a solvated electron within the SAM.

[097] The following experiments were done to confirm presence of solvated electrons in these metallic nanoparticle-SAM compositions. Magnetic force microscopy (MFM) is a sensitive tool for measuring changes in the magnetic properties of thin films, such as the increase in magnetic susceptibility that would arise from an increased concentration of unpaired, spin-½ electrons. In the MFM experiments, an atomic force microscopy cantilever with a ferromagnetic tip was scanned at a distance of 100 nm from the surface of the nanoparticle thin film, a distance at which the surface-tip interaction is determined largely by magnetic interactions. The cantilever was oscillated during the scan and changes in the oscillation frequency were measured as a phase change ($\Delta\phi$). Previous experiments and theory have established that $\Delta\phi$ is proportional to a change in the concentration of unpaired, spin-½ electrons.

[098] MFM images between two electrodes that were spaced 50 μm apart were acquired (**FIG. 3D**). This arrangement allowed exploration of changes in the film's magnetic properties as a function of voltage. When the experiment was performed in ambient conditions, the phase decreased upon applying a voltage across a film made from gold nanoparticles with TMA ligands (**FIG. 3E (Ia)**). The phase change was quantified and found that $\Delta\phi \sim -V^2$ (**FIG. 3F**). When the experiment was repeated in anhydrous conditions, no change in phase was detected. Because the chloride ions do not dissociate and migrate when the film is in the dry state, these experiments suggest that only when chloride ion vacancies are created will electrons be trapped. This control experiment rules out most other possible sources of the phase change, such as an unknown impurity within the film, the TMA ligands, or the gold nanoparticles. Films of nanoparticles having uncharged ligands such as 11-mercaptoundecanoic acid also showed no change in phase when a voltage was applied (**FIG. 3E (IIa)** and **FIG. 3F**), further indicating that a change in phase is not an inherent characteristic of ligand-stabilized gold nanoparticles. The magnetic properties of a continuous gold film were also explored (**FIG. 3E (iii)**). Even when a current was passed that was 1000 times higher than the current in the nanoparticle films, no change in phase was observed, thereby showing that the phase change in TMA nanoparticle films has a negligible contribution from magnetic induction.

[099] Since the change in phase arises from neither the gold core nor magnetic induction, the event is related to changes in the concentration of solvated, spin-½ electrons in the SAM. Quantitatively, the MFM experiments showed that the unpaired electron concentration decreases as V^2. In material systems with solvated electrons, the unpaired electrons are in equilibrium with paired electrons via the reaction

[0100] $2\ e^- \leftrightarrows ee^{2-}$ (1)

[0101] where e^- is an unpaired electron (a polaron) and ee^{2-} is an electron pair (a bipolaron, spin = 0). The mass and charge balance in this equation shows that if the unpaired electron concentration decreases as V^2, the bipolaron concentration increases as V^2. Because the material's conductivity also increases as V^2, bipolarons are the switch's *on* state and unpaired electrons are the switch's *off* state.

[0102] Referring to **FIG. 4**, when no voltage is applied, chloride anions are associated with ammonium cations. It has been established previously that electrons may exist within the SAM and can be stabilized by an image charge within the metal. Immediately after a voltage is applied (**FIG. 4A**), the capacitive movement of chloride ions between neighboring nanoparticles creates chloride vacancy sites. Each vacancy site is near an uncompensated cation, which electrostatically stabilizes an image-charge electron by localizing the electron's wavefunction near the vacancy site. Because the concentration of vacancy sites scales linearly with voltage (**FIG. 2F**), so too does the concentration of electrons (n_{e^-}) that are trapped at these sites. At these traps, the unpaired electrons are in equilibrium with bipolarons (**FIG. 4B** and equation (1)). The equilibrium constant K between unpaired and paired electrons is defined as

[0103] $$K = \frac{n_{ee^{2-}}}{n_{e^-}^2} \quad (2)$$

[0104] where $n_{ee^{2-}}$ is the concentrations of paired electrons in the traps. Because n_{e^-} grows linearly with voltage, it follows from equation (2) that $n_{ee^{2-}}$ increases as V^2. This conclusion is in exact agreement with the MFM measurements as well as the electrical conductivity measurements.

[0105] The donor-switch-acceptor model predicts that the switch's *on*, bipolaron state is lower in energy than its *off* state (**FIG. 3B**). This prediction agrees with previous studies on solvated electrons, which have shown that the free energy (ΔG) of $ee^{2-} \rightarrow 2\ e^-$ is +0.2 to +0.7 eV. This is also in agreement the inferred activation energy for $ee^{2-} \rightarrow 2\ e^-$ of

+0.9 eV (**FIG. 3A**), since the activation energy for a non-spontaneous reaction must be equal to or larger than ΔG (**FIG. 3C**).

[0106] An examination of the *j-V* characteristics for C_5, C_8, and C_{11}-TMA alkanethiols (**Fig. 2A**) reveals that when the film's resistance (*R*), is scaled by the SAM thickness (*L*), the data coincides at all voltages (**FIG. 4C**). This indicates that electron transport occurs via hopping.

[0107] Referring to **FIG. 4**, an energy diagram summarizes the model. Electron hopping through the solvated electron states indicates that the solvated electrons act as a redox couple. The oxidized form of the couple is a polaron (e^-) and the reduced form is a bipolaron (ee^{2-}). Electron transport between nanoparticles can be described according to:

[0108] $$e^-_{Au_1} + e^-_{SAM} \rightarrow ee^{2-}_{SAM} \rightarrow e^-_{Au_2} + e^-_{SAM}. \qquad (3)$$

[0109] In this process, an electron from one gold core reduces an unpaired electron within the SAM, forming a bipolaron. The paired electron species is oxidized when one of the two electrons hops to another gold nanoparticle. Like most redox couples, the equilibrium between the reduced and oxidized forms depends on temperature. Unusually, however, heating can split the reduced form into two oxidized species (equation (1)). As temperature increases, the equilibrium concentration of bipolarons decreases, limiting the rate of electron transfer to the unpaired electrons in the SAM. Within the context of the donor-switch-acceptor model, heating prevents the switch's *on* state from forming, thereby blocking electron transport.

[0110] Without being bound to any particularly theory whereby the claimed invention works, according to one preferred embodiment, the nanoparticle-based material can be thought of as being conceptually divided into two "parts:" (1) the nanoparticles themselves, which excludes the ligands and (2) the remaining volume, which includes the ligand layer but also contains several other components, such as unpaired electrons and paired electrons. A desirable aspect for paired electron formation is that there exists some non-zero concentration of electrons in the SAM when there is no applied potential. The electrons are formed within the SAM as a result of a repulsive image force between an electron that has been emitted from the metal into the SAM and the corresponding positive charge in the metal nanoparticle. If a repulsive image force between the electron and the image charge is desired, then dielectric constant of the nanoparticle is selected to be preferably less than that of the remaining volume. This aspect can therefore guide the selection of nanoparticle and ligand compositions for certain embodiments.

[0111] These materials can be thought of as a type of mesoscopic salt in which the gold nanoparticles and positively charged ligands are analogous to cations and the electrons (which are present in several forms and are accompanied by chloride ions) are the anions. Salts in which the anion is an electron are known as electrides. Consequently, these materials are the first example of a nanoparticle electride (**FIG. 4E**).

[0112] If the design aspects that are described above are met, there will exist in the remaining volume of the metallic nanoparticle-SAM material a concentration of unpaired and paired electrons. To design materials with useful concentrations of paired electrons, an important design consideration is that a large electric field be applied across the material. Optimally, fields greater than 100 V/m are applied; more optimally, fields greater than 10,000 V/m are applied; most optimally, fields greater than 100,000 V/m are applied. Applied voltages are optimally less than 30 V, and more optimally less than 5 V. The distance between electrodes (that is, the gap size over which the potential drop occurs) is optimally less than 0.5 cm, more optimally less than 0.5 mm, and most optimally less than 50 μm. In general, the design guideline is that device miniaturization leads to a higher concentration of unpaired electrons.

[0113] High conductivity is a preferred attribute of the metallic nanoparticle-SAM compositions described herein. The preferred compositions and design considerations that lead to the highest conductivity include the following features:

[0114] 1) The metallic nanoparticle should be composed primarily of a metal or degenerately-doped semiconductor or degenerately-doped insulator. The charge transport in these materials depends on the density of states in the nanoparticle core—correspondingly, the higher the density of states, the higher the tunneling electron transfer rate. Metals and degenerately-doped materials typically have higher densities of states than semiconductors. This will allow these nanoparticle-based materials to have the most significant gains in electrical conductivity, although this does not preclude the use of semiconductors for many applications.

[0115] 2) The metals that have their Fermi level closest to the peak in the density of states of the paired electrons (see **FIG. 4D**) will have the highest conductivity. Metals with work functions between 3 and 6 eV are optimal; more optimally, are metals with work functions between 4 and 5.5 eV.

[0116] 3) The shorter the ligand of formula (**Ia**), the higher the conductivity. Ligands that extend less than 2.5 nm from the nanoparticle surface are optimal; ligands that extend less than 1.5 nm from the nanoparticle surface are more optimal; ligands that extend less than 0.8 nm from the nanoparticle surface are most optimal.

[0117] 4) The salt component (**Z**) of ligand having formula (**Ia**) for the metallic nanoparticle-SAMs will provide the highest conductivity if an applied field leads to a high degree of salt dissociation. That is, the steeper the concentration gradient of ions across the device, the greater the conductivity. This is best achieved by polarizable ions that have a low enthalpy of dissociation. At the same time, the ions must be small enough to move through the remaining volume of the nanoparticle-based material. Most optimally, the anions that meet both of these criteria include chloride, bromide, iodide, nitrate, thiocyanate, acetate, and tetrafluoroborate. Most optimally, the cations that meet both of these criteria include ammonium, imidazolium, pyridinium, phosphonium, pyrazolium, pyrrolidinium, sulfonium, sulfonyl imide, piperidinium, morpholinium, and cyclopropenylium.

[0118] 5) The nanoparticle should be a composition that can survive high applied voltages. The higher the applied voltage, the higher the conductivity. Relatively stable nanoparticles include noble metals and metal oxides that have a large enthalpy of formation. Most optimally, these metal oxides include materials such as SnO_2, F-doped SnO_2, indium tin oxide (ITO), Sb-doped SnO_2, Fe_2O_3, TiO_2, MoO_3, Nb_2O_5, Ta_2O_5, or WO_3. Carbon-based materials (including carbon black, carbon nanotubes, graphene, silicon carbide, tungsten carbide, titanium carbide, and other carbides) are also highly corrosion-resistant and suitable for use herein.

[0119] 6) All of the components in the device (including the metallic nanoparticle-SAM-based material and the electrodes) should have a high capacitance. The movement of ions is limited by the material and electrode capacitance. Optimally, materials with a sufficient capacitance for this purpose include most metals. More optimally, materials with higher capacitance are preferred and are composed at least partially from components with a high dielectric constant. These can include a variety of insulators such as silica, alumina, or hafnium oxide. As explained for one embodiment, gold-silica composite electrodes are preferred to gold electrodes, because the former have superior capacitance and impart higher electrical conductivity to the nanoparticle-SAM-based material than the latter.

[0120] 7) The conductivity is maximized for small devices. As noted above, the most optimal device size provides a gap-size between electrodes of less than 50 μm. Nevertheless, these materials can readily be scaled down using common lithographic techniques. Devices with sizes on the length scale of 500 nm should be easily accessible and achieve very large gains in electrical conductivity (4 to 5 orders of magnitude improvement in electrical conductivity).

[0121] 8) The conductivity is most enhanced when the enthalpy of formation of paired

electrons is large. The paired electrons are coloumbically stabilized; the enthalpy of formation of the cation-paired electron species will scale as $Q_1 \times Q_2$, where Q_1 is the charge of the cation and Q_2 is the charge of the paired electron (that is, -2). If the cation charge is increased from +1 or +2, the enthalpy of formation of the paired electron will double. Of course, the enthalpy of the association between an unpaired electron ($Q_2 = -1$) and the +2 cation will also double. However, the magnitude of the doubling will be twice as large for the paired electron as for the unpaired electron. This leads to a relative stabilization of the bipolaron by using ligands with groups G_2 that are based on divalent cations. Such divalent cations include twice-oxidized conjugated molecules (for example, those based on polythiophene or polyacetylene). Examples of formula (**Ia**) include Polycations wherein molecules have a plurality of monovalent cations are present (for example, two alkyl ammonium ions; $\underline{b} = 2$ for formula (**Ia**)). Preferably a plurality of monovalent cations included in formula (**Ia**) include species where $\underline{b}$ is 2 to 30.

Applications

[0122] Materials with voltage-tunable electrical and magnetic properties are essential components of devices such as transistors and memory storage media. Nanoparticle electrides are the first example of a solid-state material system that dynamically traps solvated electrons. This new charge transport mechanism is amenable to deployment in miniaturized devices because the electrical conductivity increases with device miniaturization, which is a feature not typically observed in most materials. The discovery that electrons act as redox couples provides clear advances in the field of molecular electronics. Yet, the applications of these material to electronics generally would be appreciated by one skilled in the art as well with regard to the applications involving transistors, diodes, random-access memory (especially static RAM), other classes of electronic devices that are derived from transistors, varistors, thermistors, electrochromic materials (for example, materials used in active windows, displays, glasses), electromagnets, electrocatalyst, sensors, and the like.

[0123] The operation of the transistor using paired electrons generated from nanoparticle electride compositions is relatively straightforward. One set of electrodes applies a potential across the nanoparticle-based material, creating paired electrons and enhancing its conductivity. These are the gate electrodes. A second set of electrodes—the source and drain—is placed on the nanoparticle-based material in a location such that the application of the gate potential leads to no potential difference between the source and drain. Several configurations under which this condition is achieved, as shown in one preferred embodiment

in **FIG. 5A**. By maintaining a small, constant potential between the source and drain electrodes as the gate potential is increased, the current between the source and drain electrodes is increased (**FIG. 5B**). In this way, the gate potential regulates the source-drain current, enabling signal modulation and amplification. These are the key characteristics of a transistor.

[0124] A second device that relies on the unusual physical characteristics of the present materials is a thermistor. A thermistor is designed to change its resistance with temperature, effectively acting as an electrical thermometer. Thermistors are the most sensitive electrical thermometer and have achieved changes in electrical conductivity of up to 6% per degree Celsius. The nanoparticle-based materials exhibit an extraordinary change in electrical conductivity of up to 26% per degree Celsius. An illustration of the robust performance attributes of a high-performance thermistor that includes these materials is illustrated in **FIG. 5C**, where the device displays the function of resistance increasing exponentially with temperature. This makes the nanoparticle electrides the most sensitive electrical thermometer yet described.

[0125] As explained above, mixed metallic nanoparticle compositions can be prepared wherein the heterogeneous or multiphasic composition possesses modified electrical properties relative to homogeneous or monophasic compositions of formula (**Ia**). Referring to **FIG. 5D**, a diode is illustrated having a biphasic composition comprising a first monolayer of metallic nanoparticles of formula (**Ia**) in electrical communication with a second monolayer of metallic nanoparticles having a structure different from formula (**Ia**) (**FIG. 5E**). Referring to **FIG. 5F**, the resultant device displays an apparent biphasic conductivity-applied voltage relation rather than a $\sigma \sim V^2$ relation. These and other compositions fall within the scope of the applications for the disclosed metallic nanoparticle-SAM compositions of formula (**Ia**).

[0126] These materials can be prepared on flexible substrates. An example of a these materials used in a transistor-based device on a flexible substrate is illustrated in **FIG. 6.** This allows the materials to be packaged in new ways that enable a wider range of applications than traditional electronic, electrochromic, electromagnetic, or electrocatalytic materials.

[0127] The properties of these materials are extremely sensitive to the applied voltage – even when small voltages are applied, there are very significant changes in properties. This is a desirable characteristic because it implies that devices do not consume much power. The fact that multiple properties of the material are simultaneously changed when the voltage is applied may allow several novel applications to be developed in which, for example, the

ability to simultaneously tune electrical, magnetic, and optical properties is desired. The conductivity of these materials depends very sensitively on temperature. These materials can be used to build what may be among the most sensitive thermometers yet designed—they can detect changes in temperature of as little as 0.0001 °C. The magnetic properties of these materials are highly tunable and can be switches between diamagnetic, ferromagnetic, and antiferromagnetic depending on the applied potential. The sign of the photoconductivity of these materials (that is, positive indicates an increase in current with light) depends on the applied potential. This allows a single material to detect photons in multiple ways.

EXAMPLES

[0128] The invention will be more fully understood upon consideration of the following non-limiting examples, which are offered for purposes of illustration, not limitation.

Example 1. Ligand Synthesis.

[0129] *N,N,N*-trimethyl(11-mercaptoundecyl)ammonium chloride (TMA-C_{11}, **4a**), *N,N,N*-trimethyl(8-mercaptooctyl)ammonium chloride (TMA-C_8, **4b**) and *N,N,N*-trimethyl(5-mercaptopentyl)ammonium chloride (TMA-C_5, **4c**) were synthesized according to the same synthetic scheme (**FIG. 7**).

Synthesis of compounds 2a-c.

[0130] A first mixture containing sodium (400 mg (17.4 mmol)) in anhydrous methanol (15 mL) was prepared with cooling. Trimethylamine hydrochloride (1.65 g (17.3 mmol)) was added to the first mixture to form a second mixture. The second mixture was allowed to stir 5 min at RT. The corresponding bromoalkene (5 mmol; **1a-c** [**FIG. 7**]) was added to second mixture to form a third mixture. The third mixture was incubated 48 hr at RT. After this time, a first precipitate (white solid) was removed by filtration and discarded, and the filtrate of the third mixture was retained. The retained filtrate of the third mixture was concentrated and the concentrated filtrate was thereafter dissolved in methylene chloride (10 mL) to form a fourth mixture. A second precipitate that formed in the fourth mixture was removed by filtration and discarded, and the filtrate of the fourth mixture was retained. Hexane (50 mL) was added to the filtrate of the fourth mixture to produce the desired Trimethylmmoniumalkyl bromide alkene (**2a-c** [**FIG. 7**]) as a third precipitate (white solid). The third precipitate was collected and dried.

Synthesis of compounds 3a-c.

[0131] Corresponding trimethylammonium-alkyl bromide alkene (10 mmol, **2a-c** [**FIG. 7**]) was dissolved in methylene chloride (30 mL) to provide a first mixture 1. Thioacetic acid (28 mmol) and a catalytic amount of AIBN (~50 mg) were added to the first mixture to provide a

second mixture. The second mixture was UV-irradiated 7 hr at a temperature between 20 and 40 °C. The solvent of the second mixture was evaporated under vacuum and residue was triturated with dry diethyl ether (4-5 times, 50 mL) to yield crude product of thioacetyl-alkyltrimethylmmonium bromide in form of white crystals (**3a,b** [**FIG. 7**]) or dense oil (**3c** [**FIG. 7**]).

Synthesis of compounds 4a-c.

[0132] The resultant corresponding thioacetyl-alkyltrimethylmmonium bromide (**3a-c** [**FIG. 7**]) was dissolved in methanolic solution of HCl (0.1 M) to form a first mixture. The first mixture was refluxed under nitrogen for 12 hr. The first mixture was filtered, and the solvent filtrate of the first mixture was evaporated under vacuum. Crude product was dissolved in methanol (10 mL) to provide a second mixture. The second mixture was added drop-wise to well-stirred, dry diethyl ether (150 mL) to provide a third mixture having product (**4a-c**). The white precipitate (**4a**, **b**) was filtered off and dried under vacuum. Thick, pale yellow oil (**4c**) was separated by decantation of solvents from the top layer and then dried under vacuum.

Example 2. Synthesis of DDA AuNPs.

[0133] Dodecylamine-capped gold nanoparticles (DDA AuNPs) were prepared having at least one dimension of 2-4 nanometer in the following procedure. A first mixture containing $HAuCl_4 \cdot 3\ H_2O$ (47.2 mg (0.12 mmol, 1 eq.)), dodecyl amine (444.2 mg (2.396 mmol, 20 eq.)) and *N,N*-didodecyl-*N,N*-dimethylammonium bromide (554.2 mg (1.198 mmol, 10 eq.)) in toluene (13.2 mL) was prepared and sonicated for 10 min in a bath sonifier maintained at 20 to 40 °C. A second mixture containing tetrabutylammonium borohydride (117.1 mg (0.455 mmol, 3.8 eq.)) and *N,N*-didodecyl-*N,N*-dimethylammonium bromide (221.7 mg (0.479 mmol, 4 eq.)) in toluene (5.7 mL) was prepared and sonicated 10 min or until it became homogeneous. The second mixture was thereafter injected rapidly (1-5 sec) at RT into the first mixture to form a third mixture. Upon formation of the third mixture ("gold seed solution"), the color changed rapidly to dark purple. The third mixture was stirred overnight at RT.

[0134] The above procedure was modified to grow the gold nanoparticles having at least one dimension of 5.5 nm. Briefly, a first mixture containing $HAuCl_4 \cdot 3\ H_2O$ (446.1 mg (1 mmol, 1 eq.)), dodecylamine (5.248 g (28.306 mmol, 25 eq.)) and *N,N*-didodecyl-*N,N*-dimethylammonium bromide (2.095 g (4.529 mmol, 4 eq.)) in toluene (113.4 mL) was prepared. The first mixture was sonicated until it became homogeneous. A second mixture containing a gold seed solution was prepared as described above. The second mixture was introduced into the first mixture to form a third mixture. A fourth mixture

containing anhydrous hydrazine (289.9 mg (9.059 mmol, 8 eq.) and *N,N*-didodecyl-*N,N*-dimethylammonium (2.095 g (4.529 mmol, 4 eq.)) in toluene (43.8 mL) was prepared and sonicated. The fourth mixture was then added drop-wise to the third mixture over 30 min RT to form a fifth mixture. The color gradually became a more intense purple over 30 min as the fifth mixture formed. The fifth mixture was stirred overnight at RT.

Example 3. Synthesis of TMA AuNPs.

[0135] The dodecylamine ligand of 5.5 nm DDA AuNPs from Example 2 were exchanged with the TMA thiol ligand from Example 1 to provide 5.5 nm gold nanoparticles with TMA ligand (TMA AuNPs), according to the following procedure. Following overnight stirring of the fifth mixture at RT, methanol (vol. eq.) was added to the fifth mixture to form a sixth mixture to promote precipitation of the DDA AuNPs. Once the nanoparticles had precipitated from the sixth mixture, the liquid phase was removed by decantation, leaving behind a purple solid. The solid was re-dispersed in toluene (30 mL) to provide a seventh mixture. An previously-prepared eighth mixture containing TMA-C_{11} thiol (134 mg (0.5 mmol, 0.4 eq.)) in dichloromethane (20 mL) was immediately added to the seventh mixture to provide a ninth mixture. The ninth mixture, which contained the ligand exchange reaction, was allowed to proceed for three hrs, during which time the exchanged TMA AuNPs nanoparticles precipitated. The resultant TMA AuNPs nanoparticles were rinsed three times with dichloromethane (30 mL per rinse). The purified TMA AuNPs nanoparticles were subsequently dispersed in methanol (5 mL) and filtered through a 0.2 μm PVDF syringe filter. This solution was used directly to prepare devices.

Example 4. Device fabrication.

[0136] Two types of electrochemical cells were prepared that are referred to as either "gold electrodes" or "gold-silica electrodes." The gold electrodes had a low capacitance, while the gold-silica electrodes had a high capacitance.

[0137] The substrate used for all devices was a silicon wafer with a 500 nm silica thermal oxide layer. To pattern electrodes, a mask was prepared for photolithography containing the desired dimensions of the electrodes. For the two-electrode experiments, electrodes with a width of 8 mm and gap sizes of 50, 75, 100, 200 and 500 μm were patterned. The electrode length was the same as the gap size. For the four-electrode experiments, the electrode was patterned having the geometry as shown in **FIG. 2I**. For the transistor experiments, the electrode was patterned having the geometry as shown in **FIG. 5A**.

[0138] Following photolithography, the gold electrodes were deposited by e-beam evaporation of 5 nm of Cr and 40 nm of Au. Subsequently, lift-off was performed to achieve

the desired pattern. For the gold-silica electrodes, 5 nm of Cr, 40 nm of Au, and 5 nm of Cr were deposited by e-beam evaporation. Following lift-off, 100 nm of SiO_2 was evaporated onto the device using plasma-enhanced chemical vapor deposition (PECVD). The device was annealed, heating it to 700 °C over 30 minutes and holding at this temperature for 10 minutes. For all devices, gold nanoparticle films with a typical thickness of 500 nm were drop-cast from a methanol solution.

Example 5. Electrical testing.

[0139] Electrical measurements were performed in a grounded Faraday cage in the dark. Two/four electrode measurements were performed with one/two Keithley 6517 electrometers. The respective capacitances of the gold electrodes and gold-silica electrodes were measured by immersing the electrodes into 0.5 M sodium sulfate (aq.). The scan rate was 100 mV/s from 0.6 V to -0.4 V vs. Ag/AgCl. The capacitance of the gold electrode was 10 μF per cm^2 while the capacitance of gold-silica electrode was 2.2 mF per cm^2.

Example 6. Magnetic force microscopy.

[0140] Two-electrode gold-silica devices were used for the magnetic force microscopy (MFM) experiments. In the MFM experiment, a magnetized AFM tip acquired a height profile of the sample's surface. A second scan was made in which the AFM tip was moved 100 nm from the surface and the phase of the AFM tip was recorded. Changes in the phase of the oscillating cantilever correlate linearly with changes in the concentration of unpaired electrons in the sample. In particular, a decrease in phase corresponds to a decrease in the concentration of unpaired electrons.

[0141] A small, rectangular region (8 by 40 μm) of a device with a gap between electrodes of 50 μm was analyzed. For the first 4 μm of the scan, no potential was applied; for the second 4 μm, a potential ranging from 0 V to 30 V was applied. The entire scan required 4 minutes.

[0142] A control experiment involving TMA-stabilized gold nanoparticles was performed under anhydrous conditions. The experiment was performed by flowing a continuous stream of argon over the device for at least 1 hour prior to and during the MFM measurement. A home-built chamber was constructed around the AFM measurement head to assist in the creation of an anhydrous environment. The results of the MFM experiment are shown in the Table 1.

[0143]

Table 1. MFM phase vs. voltage for an anhydrous TMA gold nanoparticle film.

Voltage (V)	Change in phase (°)
0	0
5	0.07
10	0.04
15	0.59

Example 7. Secondary Ion Mass Spectrometry (SIMS).

[0144] Two-electrode devices were polarized at 5 V for 10 min. Immediately upon completing device polarization, the electrical leads were removed and the sample was transferred to an ultra-high vacuum within two minutes. By placing the sample in a high vacuum, water was rapidly removed from the nanoparticle film, thereby immobilizing the chloride ions and allowing their distribution to be probed. The Au, Cl, and S ion distributions were mapped between the two electrodes. After polarizing the electrodes for 10 minutes to reach a steady state distribution of ions, the gold:sulfur ratio remained unchanged between the electrodes as a result of the bond between the thiol ligand and the gold surface. The chlorine:gold ratio changed linearly between the two electrodes, with the highest concentration achieved at the positive electrode (anode).

[0145] The fractional gold content between polarized electrodes was analyzed to determine whether gold migration occurred. No significant gold gradient was observed (**FIG. 2G**), allowing gold to be used as a reference for estimating the migration of chlorine or sulfur (**FIG. 2 D-F**).

Example 8. Small angle x-ray scattering (SAXS).

[0146] An alternative explanation for the apparent negative activation energy (that is, a decreasing conductivity with increasing temperature) is that heating induces a lattice expansion that increases the tunneling distance between adjacent nanoparticles. To test this hypothesis, SAXS was performed on TMA-capped gold nanoparticles. The sample was cycled three times from 34 to 24 °C, which is a temperature range similar to that used in Fig.

3a. The d_{111} diffraction peak was used to determine the lattice spacing. At both 24 and 34 °C, the measured lattice spacing was 5.649 ± 0.001 nm, suggesting that thermal expansion cannot explain the apparent negative activation energy for charge transport.

Example 9. Electron Microscopy

[0147] Scanning electron microscopy was performed on the surface of the nanoparticle thin films. A representative image is shown in **FIG. 2H**.

Example 10. Four-point electrical measurements.

[0148] To accurately measure the material's electrical conductivity, nanoparticles were deposited onto a substrate with four patterned electrical contacts as illustrated in **FIGs. 2B** and **2I**. This is a relatively unusual geometry for performing four-point measurements but has an advantage compared to more traditional geometries in which the four contacts are co-linear. Because changes in the concentration of ions near an electrode surface are known to change contact resistance, passing a current between the two external electrodes induces an ion gradient (**FIG. 2E**) that changes the ion concentration at the two internal electrodes. This may modify the contact resistance at the two internal electrodes. Instead, the two sensing electrodes were oriented orthogonal to the two test electrodes and placed the sense electrodes equidistant from the test electrodes (**FIG. 2B, I**). This minimizes composition gradients at the sense electrodes as the test voltage is varied.

[0149] The observation that the material's conductivity increases in a direction that is orthogonal to the applied electric field allows several possible explanations for the non-linear *j-V* characteristics to be ruled out. These mechanisms can generally be categorized as field-assisted transport or space-charge limited transport and include models such as those described by Child's Law and the Mott-Gurney Law, as well as a Nernst-Poisson model that predicts enhanced conductivities only in the direction that the field is applied. The observation in metal nanoclusters that the electrical conductivity increases as V^2 at high fields (for example, 10 MV/m) arises because the voltage difference between adjacent nanoparticles exceeds the charging energy of the nanoparticles. The observation that the conductivity increases in an orthogonal direction to the applied field (**FIG. 2C**) as well as the fact that it occurs at much lower fields (200 to 1400 V/m in **FIG. 2C**) rules out this type of field-assisted transport.

Example 11. Evaluation of redox reactions involving atomic/molecular species to device's electrical properties.

[0150] These nanoparticle-based materials have several species that may undergo redox reactions, thereby contributing to the observed non-linear charge transport. Among the

possible oxidative half reactions are $Au^0 \rightarrow Au^{+/3+}$, $Cl^- \rightarrow Cl_2$ and $H_2O \rightarrow O_2$; among the reduction reactions are $H_2O \rightarrow H_2$ and $O_2 \rightarrow H_2O/H_2O_2$. In these films, two different half reactions may give rise to the measured current—for example, water oxidation and water reduction—thereby generating ions that contribute to an ionic current as long as water is supplied to the film.

[0151] To evaluate this possibility, the device's electrical characteristics were measured before, during and after device operation. In one experiment, the device was sealed with a thick layer of polydimethylsiloxane (PDMS) to limit the delivery of water and oxygen to the device. An amount of charge that was five times more than would be needed to electrolyze all of the water and oxygen within the device was passed through the device. No change in device performance was observed during this time. A similar experiment was performed without sealing the device. In this second experiment, an amount of charge that was more than two orders of magnitude more than that which was needed to oxidize all of the gold, chloride, and water in the film was passed through the device. Once again, device characteristics did not change during this experiment. An examination of the film's elemental composition by x-ray photoelectron spectroscopy (XPS) showed no significant loss of chlorine: the Au/Cl atomic fraction was 3.57 ± 0.19 before operation and 3.60 ± 0.22 after operation.

[0152] Besides two different half reactions, redox reactions may occur cyclically via a single half reaction—for example, chloride drifts towards the anode and is oxidized to chlorine, which then diffuses towards the cathode and is reduced—thereby allowing ionic charge transport to contribute to the current even at steady state. Because no chlorine is lost during sustained operation, it is implausible that the chloride/chlorine redox is important in these devices. Similarly, the fact that the electrical properties do not change when placed in a humidified argon environment rules out a contribution from the water/oxygen half reaction. Therefore, redox chemistry—whether occurring by two distinct half reactions or a single redox couple—cannot be used to explain the electrical characteristics of these devices

CLAIMS

The invention claimed is:

1. An electrochemical cell comprising:

a plurality of electrodes; and

an electrolyte comprising:

water content comprising from about 0.2 (vol %) to about 5.0 (vol %); and

a metallic nanoparticle-SAM composition comprising one member selected from the group having the structure of formula (**I**):

$$\underline{W}\text{-}\underline{X}_a\text{-}\underline{Y}\text{-}\underline{Z}_b \qquad \textbf{(I)},$$

wherein **W** is a metallic nanoparticle, **X** is a metallic nanoparticle-binding moiety, **Z** is a non-dissociative cationic moiety having at least one dissociative anion counterion, ***a*** is an integer selected from 1 to 4, ***b*** is an integer selected from 1 to 30, and **Y** is a linker comprising a covalent bond or a moiety radical having the structure of formula (**II**):

$$\text{-}(\mathbf{Q})_{n'}\text{-} \qquad \textbf{(II)},$$

wherein **Q** is an element radical selected from the group of elements consisting of C, N, O, P, S, Si and combinations thereof and ***n'*** is an integer selected from 1 to 30;

wherein the conductivity of said electrochemical cell decreases with increasing temperature.

2. The electrochemical cell of claim 1, wherein the metallic nanoparticle-SAM composition comprises one member selected from the group having the structure of formula (**Ia**):

$$\underline{W}\text{-}\underline{X}\text{-}\underline{Y}\text{-}\underline{Z}_b \qquad \textbf{(Ia)},$$

wherein **W** is a metallic nanoparticle, **X** is a metallic nanoparticle-binding moiety; **Z** is a non-dissociative cationic moiety having at least one dissociative anion counterion and ***b*** is an integer selected from 1 to 30; and **Y** is a linker comprising a covalent bond or a moiety radical having the structure of formula (**IIa**):

$$\text{–}(CR^1R^2)_{n'}\text{-} \qquad \textbf{(IIa)},$$

wherein R^1 and R^2 are each independently from another selected from hydrogen, halo, hydroxy, saturated or unsaturated C_{1-6} alkyl, substituted or unsubstituted C_{1-6} alkyl, saturated or unsaturated C_{1-6} alkyloxy, substituted or unsubstituted C_{1-6} alkyloxy, substituted or unsubstituted phenyl, amino, amide, ester, ether, acyl, carboxyl, keto, thiol, silyl, silyl ether, siloxyl, saturated or unsaturated heterocycle selected to contain one or more heteroatoms selected from O, S, N, P, wherein said saturated or unsaturated heterocycle is substituted with one or more substituents each independently from another selected from halo, hydroxy, saturated or unsaturated C_{1-6} alkyl, substituted or unsubstituted C_{1-6} alkyl, saturated or unsaturated C_{1-6} alkyloxy, substituted or unsubstituted C_{1-6} alkyloxy, substituted or unsubstituted phenyl, amino, amide, ester, ether, acyl, carboxyl, keto, thiol, and wherein ***n'*** is an integer from 0-30 electrolyte composition comprises either gold or silver.

3. The electrochemical cell of claim 1, wherein the metallic nanoparticle comprises a metal nanoparticle consisting of Au or Ag.

4. The electrochemical cell of claim 1, wherein the metallic nanoparticle comprises a metal oxide nanoparticle selected from the group consisting of SnO_2, F-doped SnO_2, indium tin oxide (ITO), Sb-doped SnO_2, Fe_2O_3, TiO_2, MoO_3, Nb_2O_5, Ta_2O_5, or WO_3.

5. The electrochemical cell of claim 1, wherein the metallic nanoparticle comprises a carbon-based material selected from the group consisting of carbon black, fullerenes, carbon nanotubes, graphene and metal carbides.

6. The electrochemical cell of claim 1, wherein the metallic nanoparticle has at least one dimension in the range from about 1 nm to about 100 nm.

7. The electrochemical cell of claim 1, wherein the **Y-Z** has a combined length less than or equal to about 2.5 nm.

8. The electrochemical cell of claim 2, wherein the **Y** consists of a member selected from the group consisting of a covalent bond or a moiety radical having the structure of formula (**IIa**):

$$-(CR^1R^2)_n- \qquad \textbf{(IIa)},$$

wherein R^1 and R^2 are each H, and ***n*** is selected from 4, 5, 6, 7, 8, 9, 10 11 and 12.

9. The electrochemical cell of claim 1, wherein:

the non-dissociative cationic moiety selected from the group consisting of ammonium, imidazolium, pyridinium, phosphonium, pyrazolium, pyrrolidinium, sulfonium, sulfonyl imide, piperidinium, morpholinium, and cyclopropenylium; or

the dissociative anion counterion is selected from the group consisting of chloride, bromide, iodide, nitrate, thiocyanate, acetate, and tetrafluoroborate.

10. The electrochemical cell of claim 1, wherein electrochemical cell exhibits non-linear conductivity versus voltage bahavior in response to an applied voltage.

11. Use of the electrochemical cell of claim 1 in a device configured to operate within a range of relative humidity from about 20% to about 80%, wherein the device is selected from a transistor and a thermistor.

12. A nanoscale switch comprising:

an electrolyte composition comprising:

a nanoparticle composition, comprising:

a metallic nanoparticle, and

a ligand having a non-dissociative cationic moiety and a dissociative anion counterion moiety,

wherein the ligand is coupled to the metallic nanoparticle; and

a water content comprising from about 0.2 (vol %) to about 5.0 (vol %);

wherein nanoparticle composition is configured to switch between a first state and a second state, wherein electron movement in the nanoparticle composition is permitted when the switch is in the first state and wherein electron movement in the nanoparticle composition is not permitted when the switch is in the second state.

13. A nanoscale switch of claim 12, wherein the nanoparticle composition is selected from a member of the group having the structure of formula (**Ia**):

$$W\text{-}X\text{-}Y\text{-}Z_b \qquad \textbf{(Ia)},$$

wherein **W** is a metallic nanoparticle, **X** is a metallic nanoparticle-binding moiety; **Z** is a non-dissociative cationic moiety having at least one dissociative anion counterion and ***b*** is an integer selected from 1 to 30; and **Y** is a linker comprising a covalent bond or a moiety radical having the structure of formula (**IIa**):

$$-(CR^1R^2)_{n'}- \qquad \textbf{(IIa)},$$

wherein R^1 and R^2 are each independently from another selected from hydrogen, halo, hydroxy, saturated or unsaturated $C_{1\text{-}6}$ alkyl, substituted or unsubstituted $C_{1\text{-}6}$ alkyl, saturated or unsaturated $C_{1\text{-}6}$ alkyloxy, substituted or unsubstituted $C_{1\text{-}6}$ alkyloxy, substituted or unsubstituted phenyl, amino, amide, ester, ether, acyl, carboxyl, keto, thiol, silyl, silyl ether, siloxyl, saturated or unsaturated heterocycle selected to contain one or more heteroatoms selected from O, S, N, P, wherein said saturated or unsaturated heterocycle is substituted with one or more substituents each independently from another selected from halo, hydroxy, saturated or unsaturated $C_{1\text{-}6}$ alkyl, substituted or unsubstituted $C_{1\text{-}6}$ alkyl, saturated or unsaturated $C_{1\text{-}6}$ alkyloxy, substituted or unsubstituted $C_{1\text{-}6}$ alkyloxy, substituted or unsubstituted phenyl, amino, amide, ester, ether, acyl, carboxyl, keto, thiol, and wherein ***n'*** is an integer from 0-30 electrolyte composition comprises either gold or silver.

14. The nanoscale switch of claim 13, wherein the metallic nanoparticle comprises Au or Ag.

15. The nanoscale switch of claim 13, wherein the metallic nanoparticle comprises a metal oxide selected from the group consisting of SnO_2, F-doped SnO_2, indium tin oxide (ITO), Sb-doped SnO_2, Fe_2O_3, TiO_2, MoO_3, Nb_2O_5, Ta_2O_5, or WO_3.

16. The nanoscale switch of claim 13, wherein the metallic nanoparticle comprises a carbon-based material selected from the group consisting of carbon black, fullerenes, carbon nanotubes, graphene and metal carbides.

17. The nanoscale switch of claim 13, wherein the metallic nanoparticle has at least one dimension in the range from about 1 nm to about 100 nm.

18. The nanoscale switch of claim 13, wherein the **Y-Z** has a combined length less than or equal to about 2.5 nm.

19. The nanoscale switch of claim 13, wherein the **Y** consists of a member selected from the group consisting of a covalent bond or a moiety radical having the structure of formula (**IIa**):

$$-(CR^1R^2)_n- \qquad \textbf{(IIa)},$$

wherein R^1 and R^2 are each H, and ***n*** is selected from 4, 5, 6, 7, 8, 9, 10 11 and 12.

20. The nanoscale switch of claim 13, wherein:

the non-dissociative cationic moiety selected from the group consisting of ammonium, imidazolium, pyridinium, phosphonium, pyrazolium, pyrrolidinium, sulfonium, sulfonyl imide, piperidinium, morpholinium, and cyclopropenylium; or

the dissociative anion counterion is selected from the group consisting of chloride, bromide, iodide, nitrate, thiocyanate, acetate, and tetrafluoroborate.

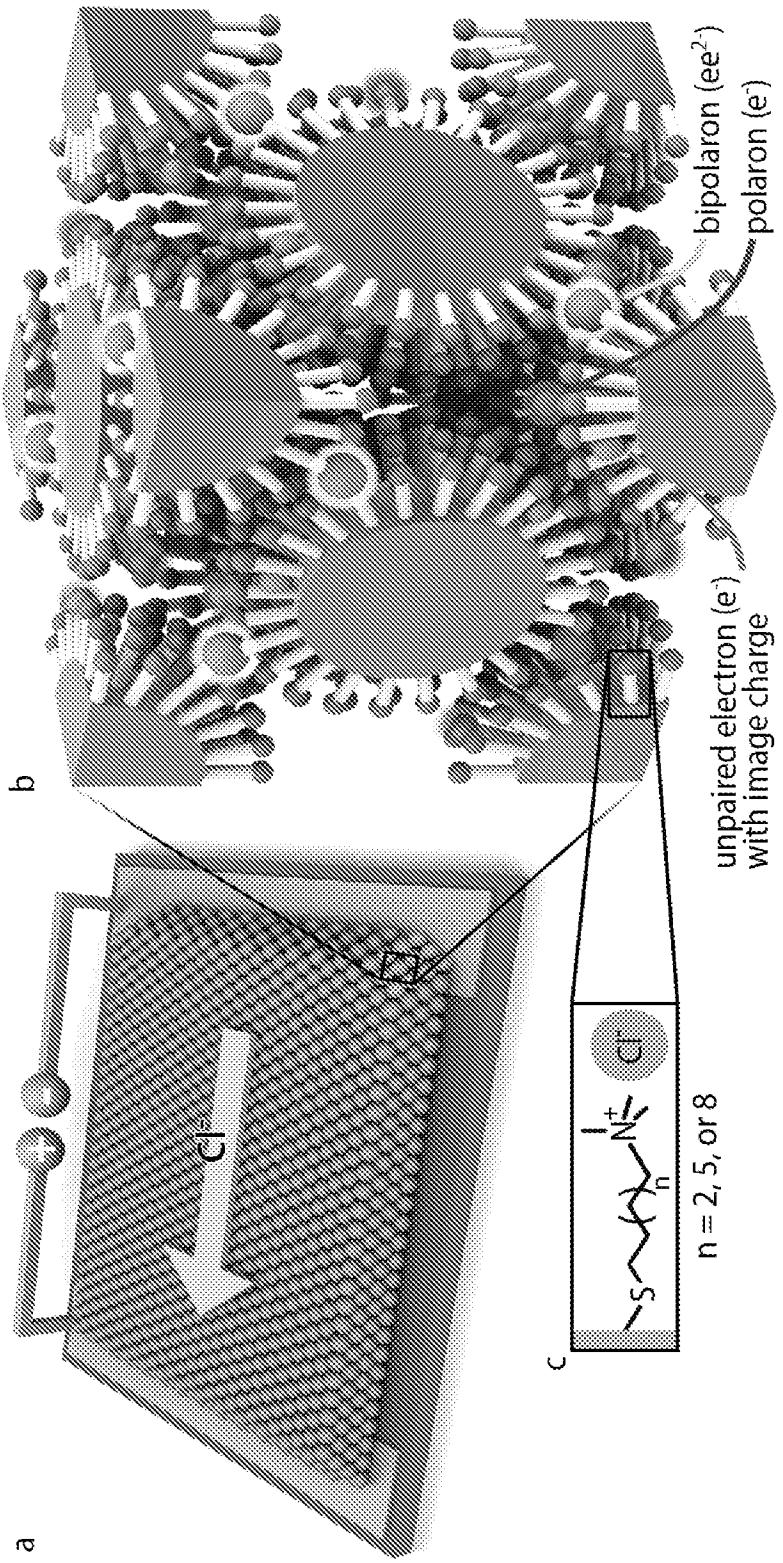
a
b
c
Cl⁻
bipolaron (ee⁻²)
polaron (e⁻)
unpaired electron (e⁻)
with image charge
Cl⁻
n = 2, 5, or 8

FIG. 1 (A-C)

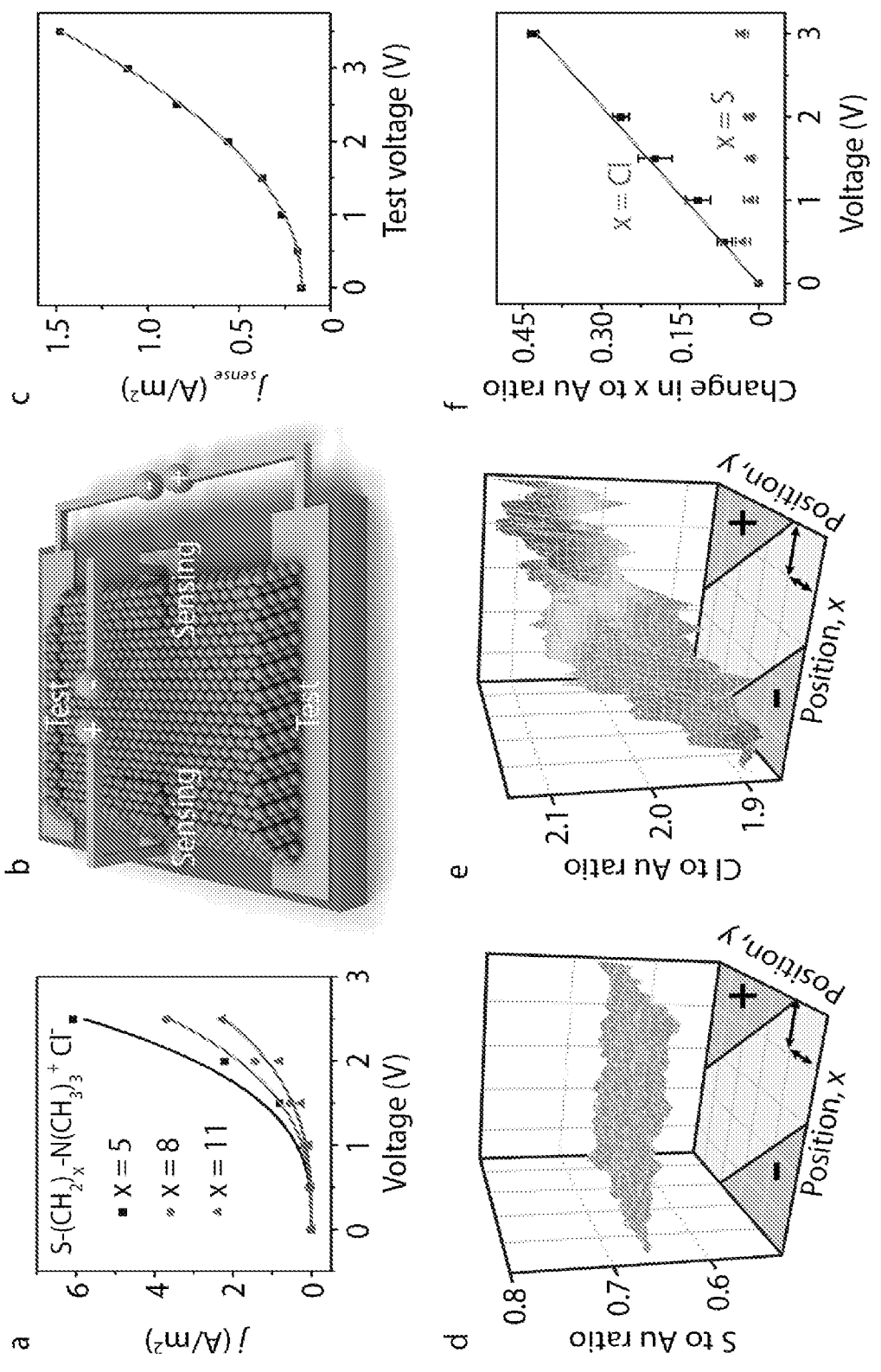
a
S-(CH2)x-N(CH3)3+ Cl-
x = 5
x = 8
x = 11
j (A/m2)
Voltage (V)
b
Test
Sensing
Sensing
Test
c
jsense (A/m2)
Test voltage (V)
d
S to Au ratio
Position, x
Position, y
e
Cl to Au ratio
Position, x
Position, y
f
Change in x to Au ratio
x = Cl
x = S
Voltage (V)

FIG. 2 (A-F)

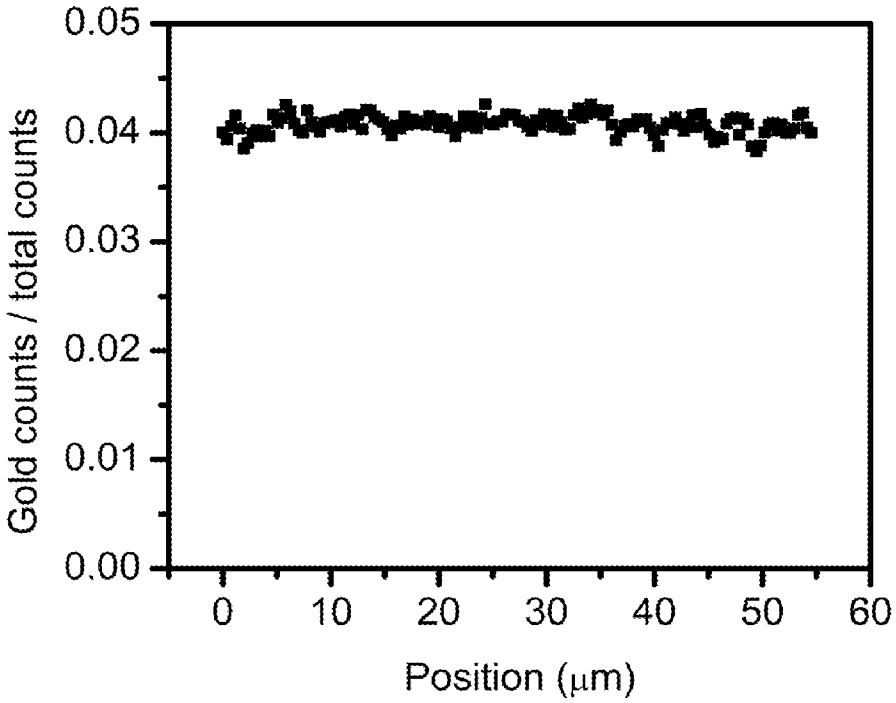
0.05
0.04
0.03
0.02
0.01
0.00
Gold counts / total counts
0
10
20
30
40
50
60
Position (μm)

FIG. 2 (G)

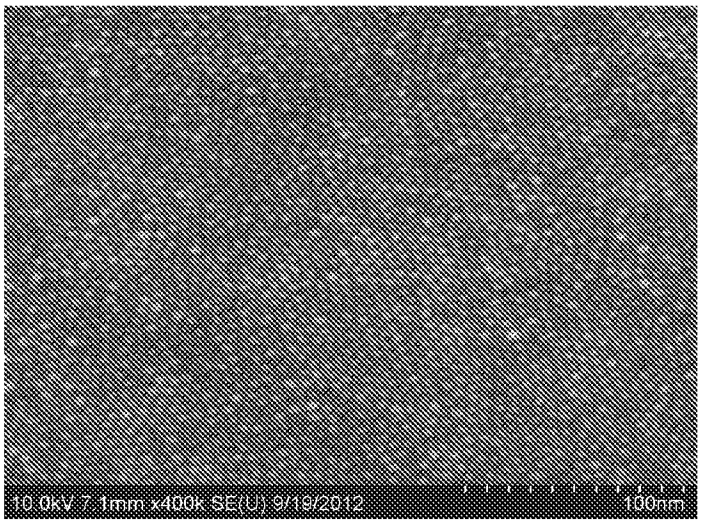
10.0kV 7.1mm x400k SE(U) 9/19/2012
100nm

FIG. 2 (H)

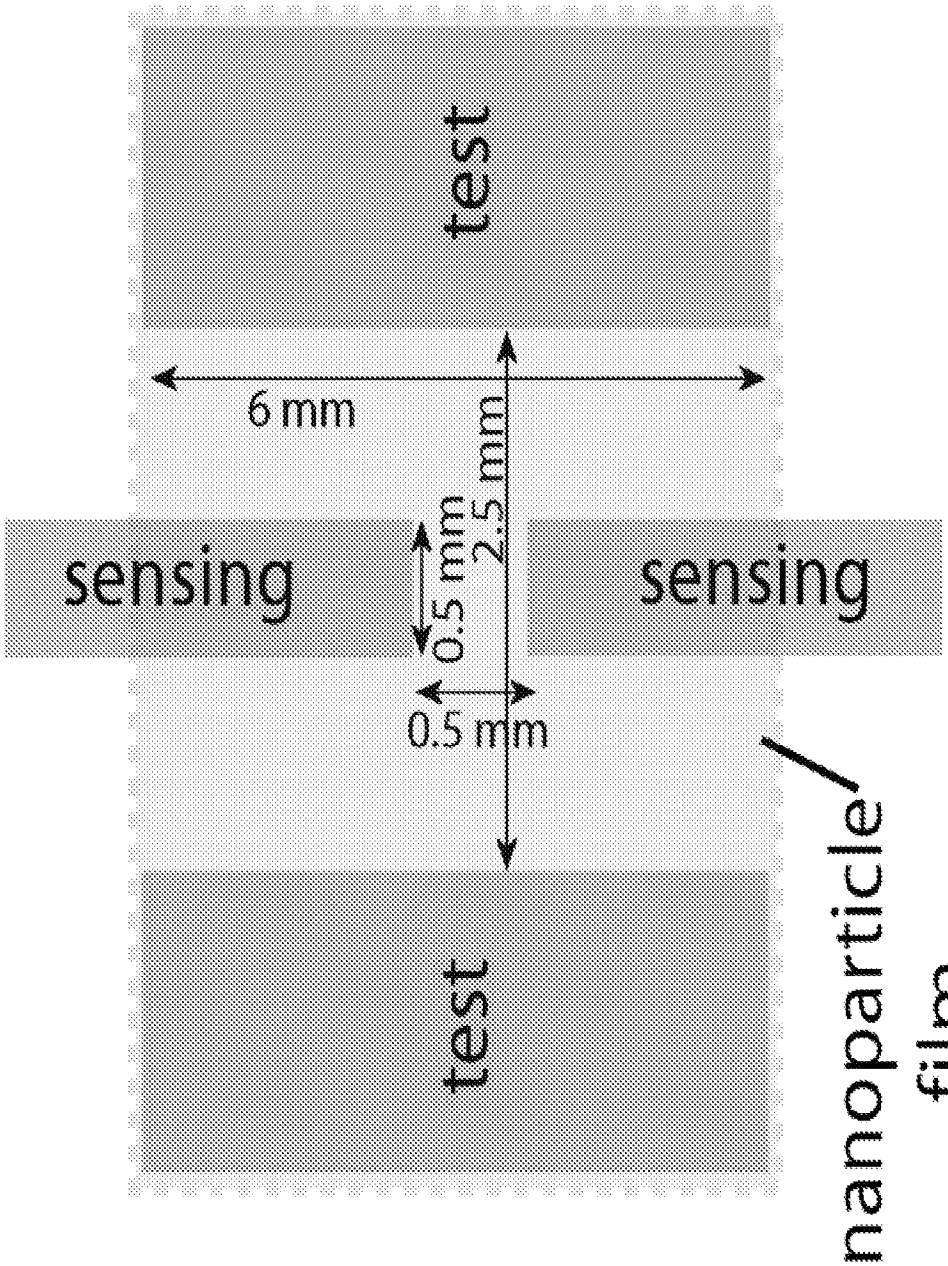
test
6 mm
2.5 mm
sensing
0.5 mm
sensing
0.5 mm
test
nanoparticle
film

FIG. 2 (I)

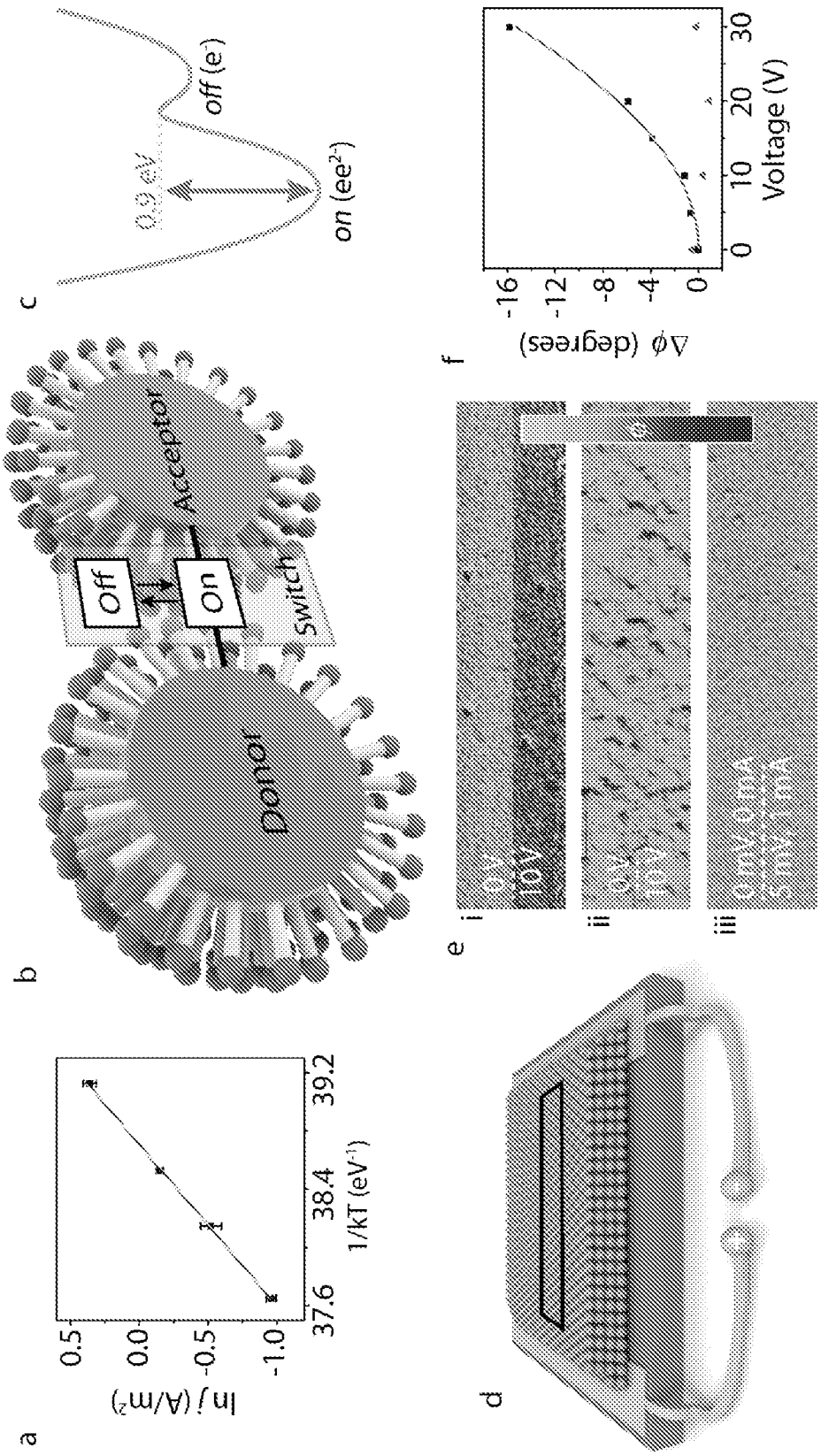
a
ln j (A/m²)
0.5
0.0
-0.5
-1.0
37.6
38.4
39.2
1/kT (eV⁻¹)
b
Off
On
Switch
Acceptor
Donor
c
0.9 eV
off (e)
on (ee²⁻)
d
e
i
0V
10V
ii
9V
10V
iii
0 mM 0.8mA
5mM 1mA
f
Δφ (degrees)
-16
-12
-8
-4
0
0
10
20
30
Voltage (V)

FIG. 3 (A-F)

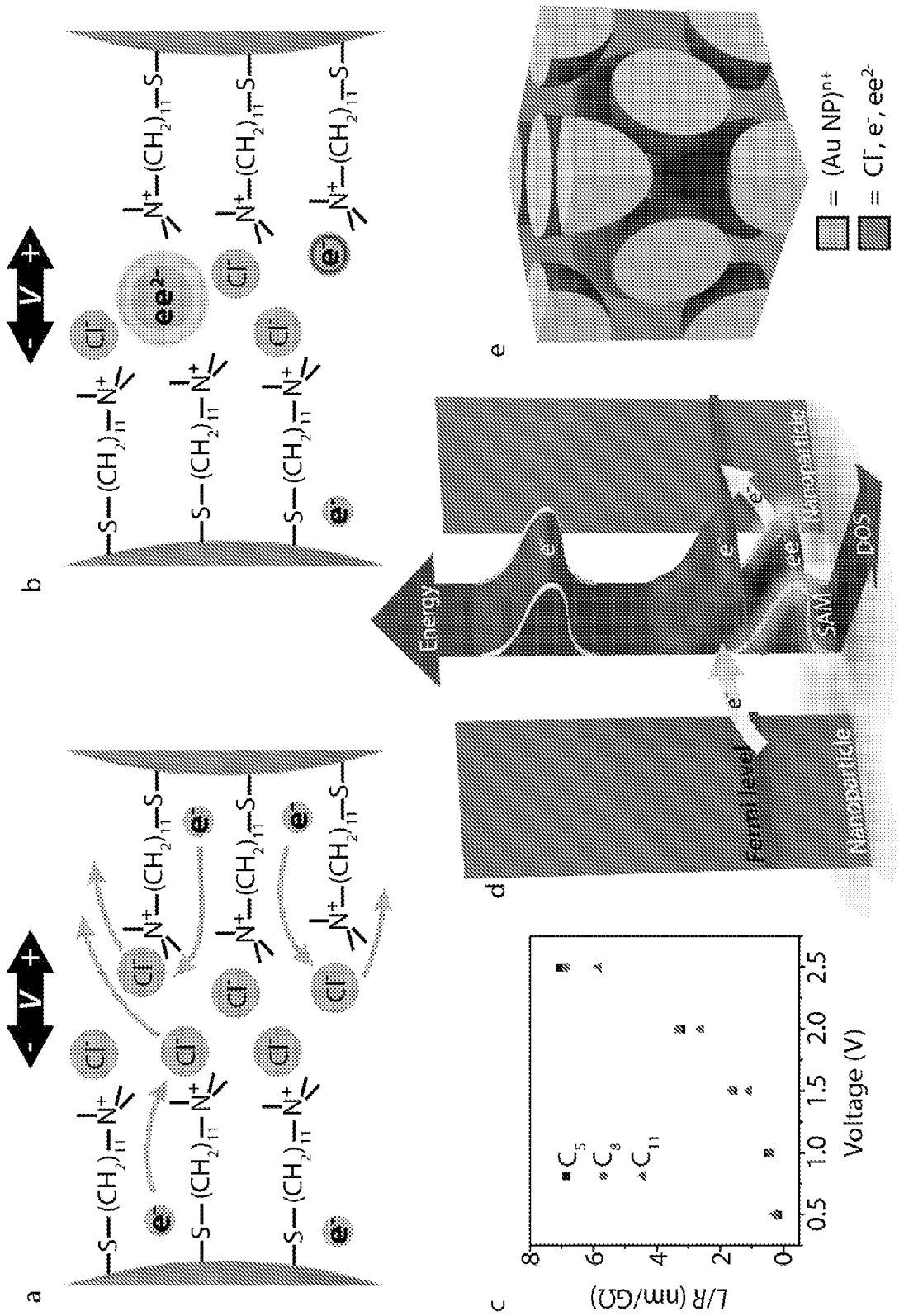
a
b
c
d
e
V
Cl⁻
e⁻
ee²⁻
Energy
Fermi level
Nanoparticle
SAM
Electrode
L/R (nm/GΩ)
Voltage (V)
C5
C8
C11
= (Au NP)n+
= Cl⁻, e⁻, ee²⁻

FIG. 4 (A-F)

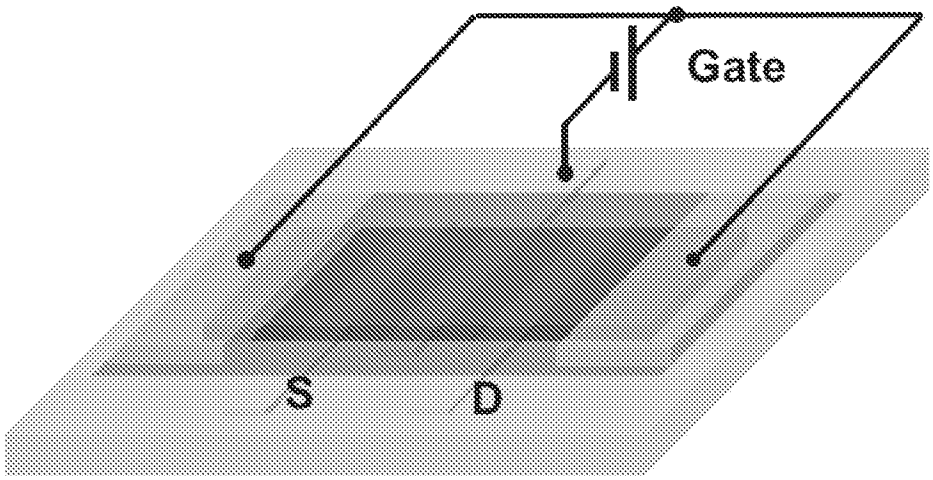
Gate
S
D

FIG. 5 (A)

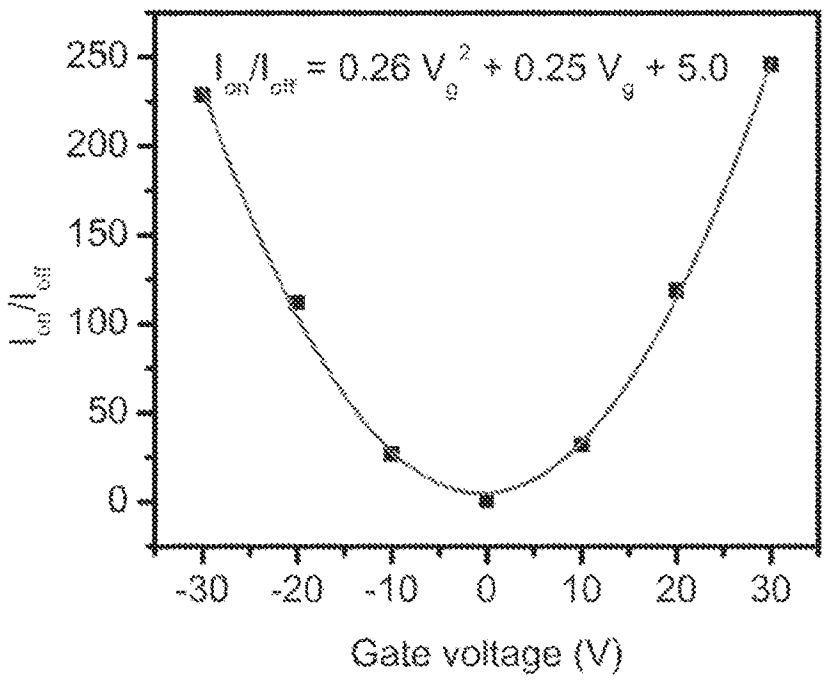
$I_{on}/I_{off} = 0.26\ V_g^2 + 0.25\ V_g + 5.0$
I_{on}/I_{off}
250
200
150
100
50
0
-30
-20
-10
0
10
20
30
Gate voltage (V)

FIG. 5 (B)

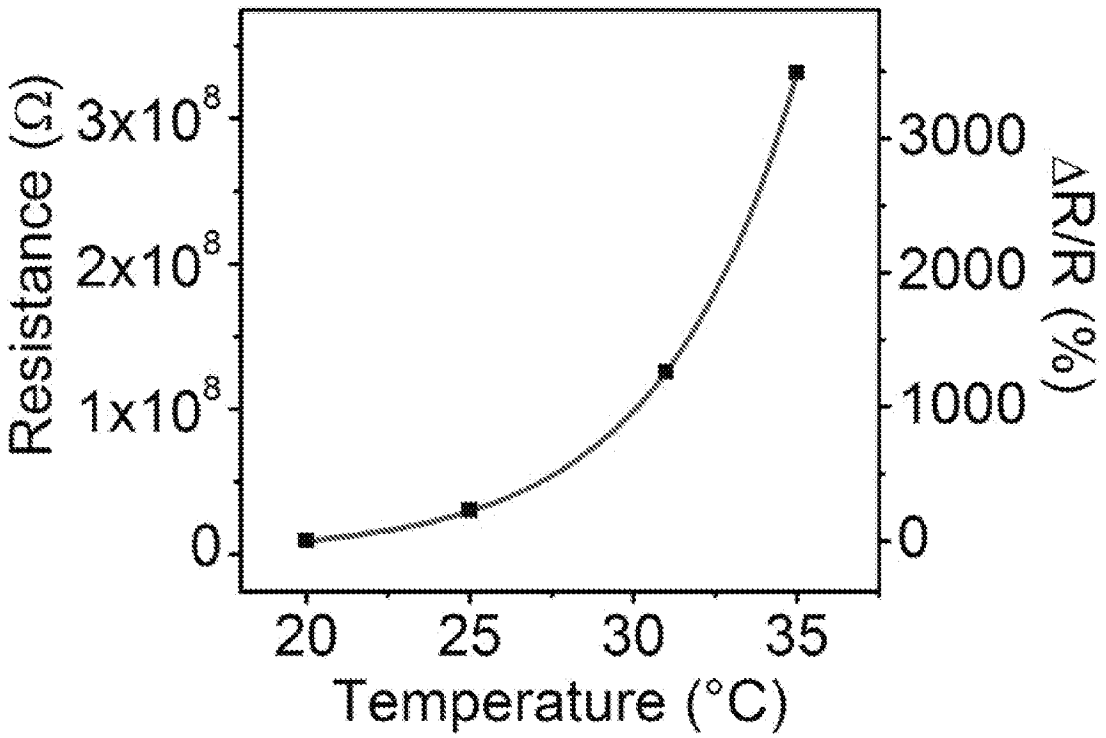
Resistance (Ω)
3x10^8
2x10^8
1x10^8
0
3000
2000
1000
0
ΔR/R (%)
20
25
30
35
Temperature (°C)

FIG. 5 (C)

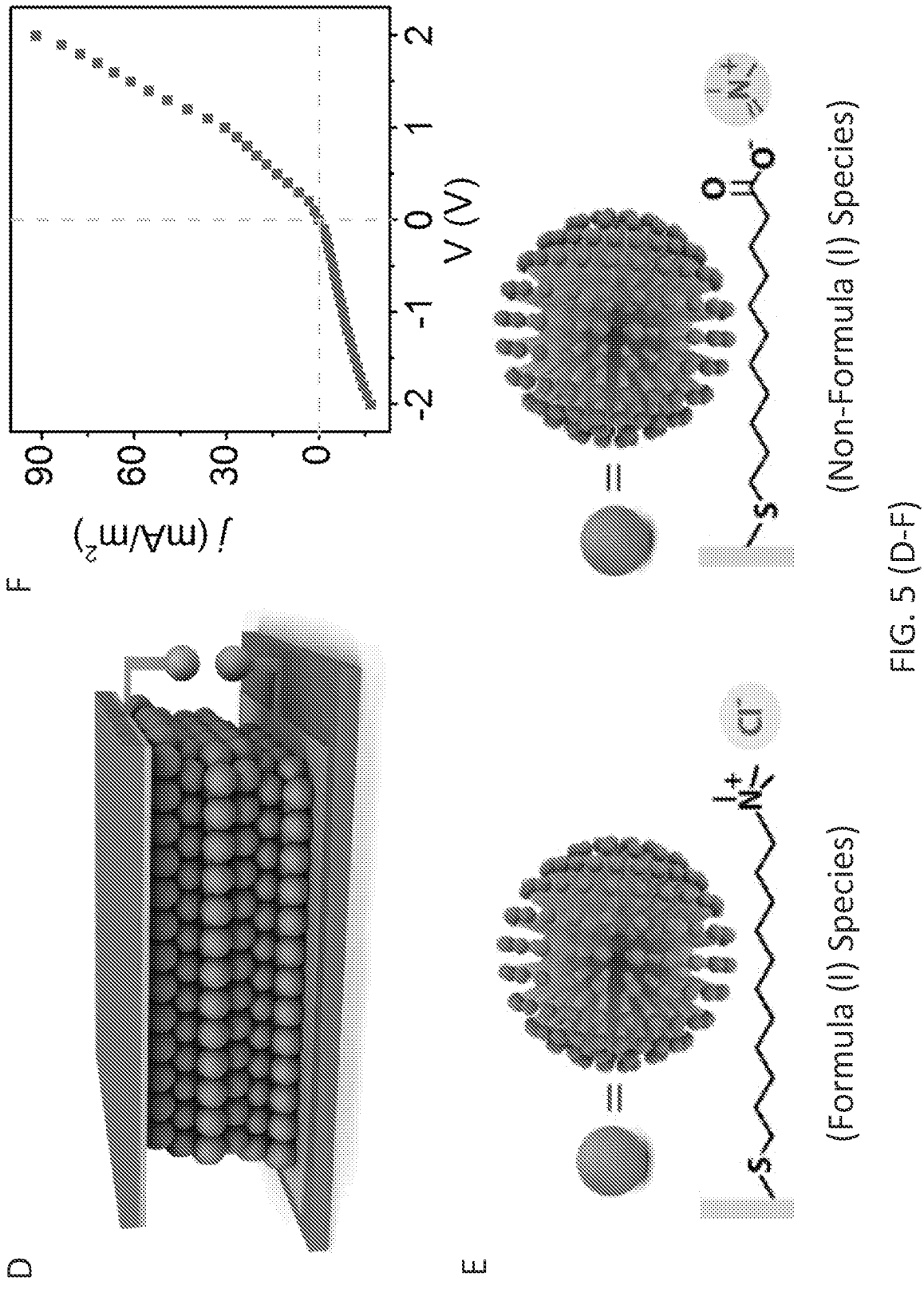
F
j (mA/m²)
90
60
30
0
-2
-1
0
1
2
V (V)
E
(Non-Formula (I) Species)
(Formula (I) Species)
Cl⁻
D

FIG. 5 (D-F)

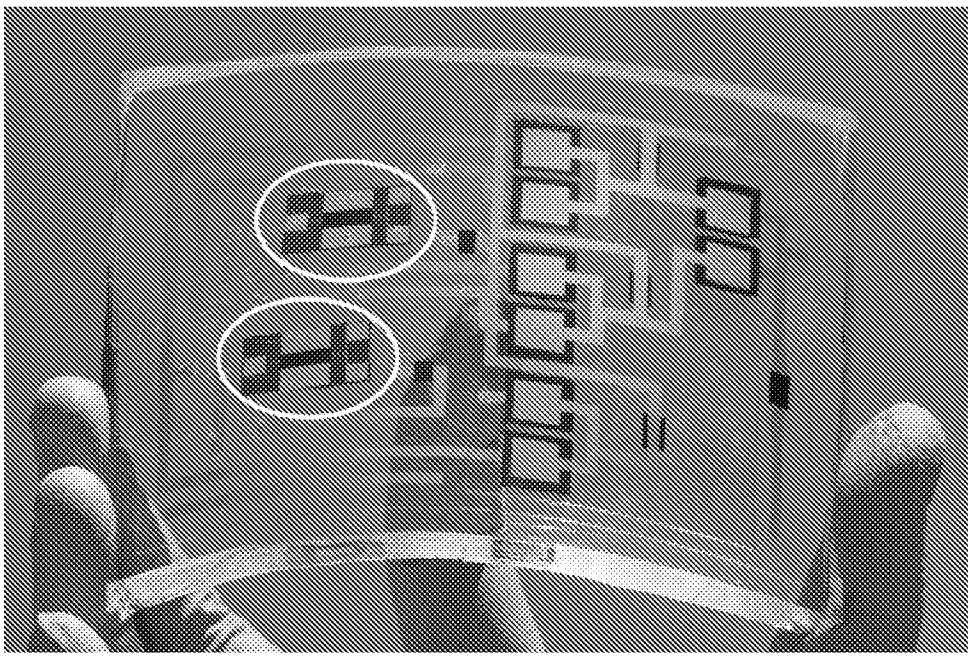

FIG. 6

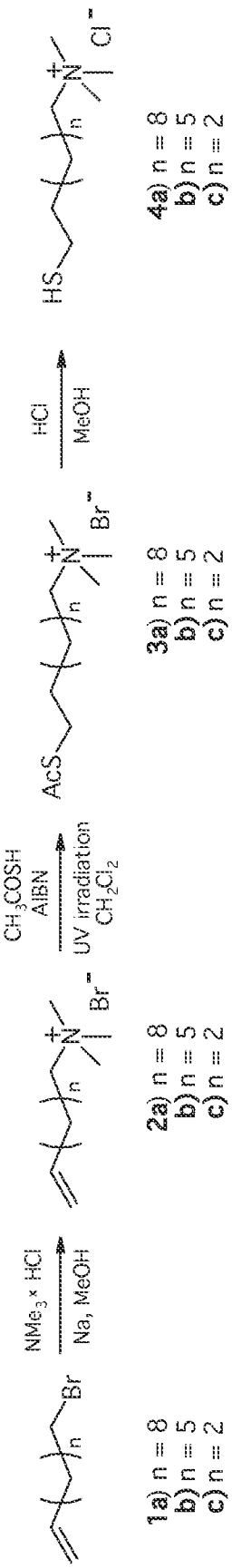
1a) n = 8
b) n = 5
c) n = 2
Br
n
NMe3 x HCl
Na, MeOH
2a) n = 8
b) n = 5
c) n = 2
Br⁻
CH3COSH
AIBN
UV irradiation
CH2Cl2
3a) n = 8
b) n = 5
c) n = 2
AcS
Br⁻
HCl
MeOH
4a) n = 8
b) n = 5
c) n = 2
HS
Cl⁻

FIG. 7

INTERNATIONAL SEARCH REPORT

International application No
PCT/US2013/040451

A. CLASSIFICATION OF SUBJECT MATTER
INV. H01M6/04 H01L39/22
ADD.

According to International Patent Classification (IPC) or to both national classification and IPC

B. FIELDS SEARCHED

Minimum documentation searched (classification system followed by classification symbols)
H01M H01L

Documentation searched other than minimum documentation to the extent that such documents are included in the fields searched

Electronic data base consulted during the international search (name of data base and, where practicable, search terms used)
EPO-Internal, WPI Data

C. DOCUMENTS CONSIDERED TO BE RELEVANT

Category*	Citation of document, with indication, where appropriate, of the relevant passages	Relevant to claim No.
X	HIDEYUKI NAKANISHI ET AL: "Dynamic internal gradients control and direct electric currents within nanostructured materials", NATURE NANOTECHNOLOGY, vol. 6, no. 11, 16 October 2011 (2011-10-16), pages 740-746, XP055083276, ISSN: 1748-3387, DOI: 10.1038/nnano.2011.165	1-3, 6-14, 17-20
Y	page 740 - page 745; figures 1,2	4,5,15, 16
	----- -/--	

[X] Further documents are listed in the continuation of Box C.

[X] See patent family annex.

* Special categories of cited documents :

"A" document defining the general state of the art which is not considered to be of particular relevance

"E" earlier application or patent but published on or after the international filing date

"L" document which may throw doubts on priority claim(s) or which is cited to establish the publication date of another citation or other special reason (as specified)

"O" document referring to an oral disclosure, use, exhibition or other means

"P" document published prior to the international filing date but later than the priority date claimed

"T" later document published after the international filing date or priority date and not in conflict with the application but cited to understand the principle or theory underlying the invention

"X" document of particular relevance; the claimed invention cannot be considered novel or cannot be considered to involve an inventive step when the document is taken alone

"Y" document of particular relevance; the claimed invention cannot be considered to involve an inventive step when the document is combined with one or more other such documents, such combination being obvious to a person skilled in the art

"&" document member of the same patent family

Date of the actual completion of the international search	Date of mailing of the international search report
10 October 2013	17/10/2013

Name and mailing address of the ISA/	Authorized officer
European Patent Office, P.B. 5818 Patentlaan 2 NL - 2280 HV Rijswijk Tel. (+31-70) 340-2040, Fax: (+31-70) 340-3016	Panitz, J

INTERNATIONAL SEARCH REPORT

International application No
PCT/US2013/040451

C(Continuation). DOCUMENTS CONSIDERED TO BE RELEVANT

Category*	Citation of document, with indication, where appropriate, of the relevant passages	Relevant to claim No.
Y	GUBIN S P ET AL: "Promising avenues of research in nanoscience: chemistry of semiconductor nanoparticles", RUSSIAN CHEMICAL BULLETIN, KLUWER ACADEMIC PUBLISHERS-PLENUM PUBLISHERS, NE, vol. 54, no. 4, 1 April 2005 (2005-04-01), pages 827-852, XP019224605, ISSN: 1573-9171, DOI: 10.1007/S11172-005-0331-3 pages 843-844	4,5,15, 16
A	US 2010/237325 A1 (SARAF RAVI F [US] ET AL) 23 September 2010 (2010-09-23) the whole document	1-20

INTERNATIONAL SEARCH REPORT

Information on patent family members

International application No
PCT/US2013/040451

Patent document cited in search report	Publication date	Patent family member(s)	Publication date
US 2010237325 A1	23-09-2010	NONE	